Shi, B.; Mosler, J.:

On the macroscopic description of yield surface evolution by means of distortional hardening models: Application to magnesium

In: International Journal of Plasticity (2012) Elsevier

DOI: 10.1016/j.ijplas.2012.11.007

On the macroscopic description of texture evolution by means of distortional hardening models: application to magnesium

Baodong Shi[a], Jörn Mosler[a,b,*]

[a] *Helmholtz-Zentrum Geesthacht, Institute of Materials Research, Materials Mechanics, D-21502 Geesthacht, Germany*

[b] *TU Dortmund, Institute of Mechanics, Leonhard-Euler-Straße 5, D-44227 Dortmund, Germany*

Abstract

Texture evolution in polycrystals due to rotation of the atomic lattice in single grains results in a complex macroscopic mechanical behavior which cannot be reasonably captured only by classical isotropic or kinematic hardening in general. More precisely and focusing on standard rate-independent plasticity theory, the complex interplay at the microscale of a polycrystal leads to an evolving macroscopic anisotropy of the yield surface, also known as distortional or differential hardening. This effect is of utmost importance, if non-radial loading paths such as those associated with forming processes are to be numerically analyzed. In the present paper, different existing distortional hardening models are critically reviewed. For a better comparison, they are reformulated into the modern framework of hyperelastoplasticity, and the same objective time derivative is applied to all evolution equations. Furthermore, since the original models are based on a Hill-type yield function not accounting for the stress differential effect as observed in hcp metals such as magnesium, respective generalizations are also discussed. It is shown that only one of the resulting models can fulfill the second law of thermodynamics. That model predicts a high curvature of the yield function in loading direction, while the opposite region of the yield function is rather flat. Indeed, such a response can be observed for some materials such as aluminum alloys. In the case of magnesium, however, that does not seem to be true. Therefore, a novel constitutive model is presented. Its underlying structure is comparably simple and the model is thermodynamically consistent. Conceptually, distortional hardening is described by an Armstrong-Frederick-type evolution equation. The predictive capabilities of the final model are demonstrated by comparisons

*Corresponding author. Tel.: +49 231 755 5744
URL: joern.mosler@udo.edu (Jörn Mosler)

to experimentally measured data.

Keywords: Distortional hardening; differential hardening; finite strain plasticity theory; texture evolution

---

1. Introduction

Although much effort has already been made to understand the macroscopic mechanical response of metallic polycrystals, this topic remains to be one of the most active research areas in constitutive modeling. For a recent overview, the reader is referred to Miehe et al. (2002) and references cited therein. Probably the most difficult problem associated with a macroscopic description of polycrystals is to capture the complex interplay at the microscale, i.e., the evolution of the microstructure, see e.g. Homayonifar and Mosler (2011, 2012). This complex interplay at the microscale, in turn, leads to a complex mechanical response at the macroscale, cf. Miehe et al. (2002). Focusing on phenomenological rate-independent plasticity models, the evolution of the microstructure yields, for instance, an evolving anisotropy of the material. This manifests in the so-called *cross hardening effect* after orthogonal loading-path changes, see Hiwatashi et al. (1998); Wang et al. (2006). Accordingly, whenever strain path changes occur, which is the case in almost every technologically relevant process such as deep-drawing, the distortion of the macroscopic yield function has to be accounted for and, thus, classical macroscopic isotropic or kinematic hardening models are not sufficient anymore, cf. Noman et al. (2010); Boers et al. (2010).

Since the macroscopic mechanical response of metallic polycrystals is a direct consequence of the underlying microstructure, a multiscale description seems to be promising. Indeed, several researchers have advocated such a modeling approach, cf. Miehe et al. (2002) and references cited therein. Most frequently, crystal plasticity theory is employed at the microscale, cf. Miehe et al. (2002); Homayonifar and Mosler (2012); Fernandez et al. (2011); Choi et al. (2011); Ma et al. (2012); Neil and Agnew (2009). By considering a representative volume element (RVE), the transition to the macroscale is realized by a certain homogenization method, see. Miehe et al. (2002). Although such methods are conceptually relatively simple, they result in high computational complexity. This is even true, if comparably crude approximations such as those known from the mean-field-theory-based self-consistent approaches (Lebensohn et al., 2004) or the Taylor model (Miehe and Rosato, 2007) are made.

A direct macroscopic phenomenological description provides an alternative to the aforementioned multiscale approaches. Clearly, such a description is computationally more efficient and thus, can be directly applied to the analysis of large-scale engineering problems. However, the numerical efficiency comes along with a coarser

resolution concerning the underlying microstructure. For instance, the plastic deformation within a certain grain cannot be predicted by a purely macroscopic model. Clearly, this is not surprising, since the macroscopic approach can be understood as a projection (homogenization) of some microscopic model. Since the final goal pursued by the authors is the modeling of large-scale forming processes of magnesium sheets, a direct macroscopic phenomenological description is considered here. To be more explicit, the framework of rate-independent finite strain plasticity is adopted.

Evidently, a macroscopic phenomenological description of magnesium has to capture the most relevant mechanical properties of this metal. Such properties encompass the stress differential effect (different yield stress in tension and compression; abbreviated as SD-effect in what follows), the material's initial anisotropy resulting from the underlying atomic lattice (hcp in case of magnesium) as well as the evolving material's anisotropy due to evolution of the microstructure, cf. Christian and Mahajan (1995). Concerning the SD-effect, Drucker-type yield surfaces are usually employed, see Cazacu and Barlat (2004). In contrast to the classical von Mises yield function, they also include the third invariant of the deviatoric stress tensor. Such yield surfaces can be extended to anisotropic materials in a standard manner, e.g. by introducing structural tensors (see Johansson et al. (2005); Vladimirov et al. (2010)) or by applying a linear transformation to the stress tensor, see Barlat et al. (2005, 2007). In summary, the SD-effect as well as the initial anisotropy can be captured in a relatively straightforward manner by existing models.

In contrast to the SD-effect and the initial anisotropy, modeling the evolution of the microstructure from a macroscopic point of view is comparably difficult. To be more precise, only few approaches have been published in this connection, see e.g. Hiwatashi et al. (1998); Haddadi et al. (2006); Feigenbaum and Dafalias (2007, 2008); Boers et al. (2010); Noman et al. (2010); Pietryga et al. (2012). Essentially, two significantly different evolution mechanisms have to be distinguished: grain refinement and coarsening on the one hand and dislocation structures on the other hand. As discussed in Wang et al. (2008), the latter is the major driving source in sheet forming processes. Since the modeling of such processes for magnesium is the overriding goal pursued by the authors, the focus is exactly on the effect of dislocation structures on the resulting macroscopic mechanical response.

In the present paper, three different phenomenological macroscopic models suitable for the analysis of texture evolution due to dislocation structures are critically analyzed first. Models in which the distortion of the yield function is only driven by the accumulated plastic strain such as those proposed in Plunkett et al. (2006); Mekonen et al. (2012) are not considered here, since they cannot predict a loading-path-dependent evolution of the yield function.

The first distortional hardening model analyzed in the present paper was published in a series of papers by Teodosiu and co-workers, cf. Hiwatashi et al. (1998); Li et al. (2003); Haddadi et al. (2006)). For this reason, the following is referred to as the *Teodosiu model*. Although such models do not capture the evolving distortion of the macroscopic yield function, they do account for the cross hardening effect. That is realized by adding another isotropic-like hardening term and by modifying the evolution equation driving kinematic hardening. In contrast to conventional models, both terms also depend on the loading direction. Even though the cited models can partly predict the effect of dislocation structures, focus seems to be on a precise modeling of work hardening stagnation, work softening and resumption. For a critical analysis of the Teodosiu model, the interested reader is referred to Wang et al. (2008). Within the cited paper it was shown that the original Teodosiu model is mathematically ill-posed and thus, has to be modified. Without going into too much detail, the equation defining the evolving anisotropy have to be slightly adjusted for that reason.

An alternative description for the macroscopic modeling of texture evolution due to dislocation structures was advocated by Levkovitch & Svendsen, cf. Barthel et al. (2008); Noman et al. (2010) and therefore referred to as *Levkovitch-Svendsen model* in the following. In line with the Teodosiu model, the initial anisotropy is captured by a Hill-type yield function. However and in contrast to Haddadi et al. (2006), the respective fourth-order tensor defining the material's symmetry is not kept constant, but evolves in time. By doing so, the shape of the resulting yield function is implicitly deformation-dependent and cross hardening is naturally included in the model. Although the Levkovitch & Svendsen model is well motivated from a physics point of view, it has not been derived from thermodynamical principles. For this reason, it is not clear, if it fulfills the second law of thermodynamics.

A model strictly complying with the second law of thermodynamics was recently proposed in Feigenbaum and Dafalias (2007, 2008); Plesek et al. (2010). According to the authors of the cited papers, this model is referred to as *Feigenbaum & Dafalias model*. Although it shares some similarities with the Levkovitch & Svendsen model, it shows one fundamental difference. This difference is the strong coupling between kinematic and distortional hardening which leads to a high curvature increase of the yield function in loading direction, while the opposite region of the yield function is rather flat. Indeed, this can be observed in experiments for some polycrystalline metals (see Feigenbaum and Dafalias (2007)). However, counterexamples have also been reported, cf. Wang et al. (2008). Finally, it has to be mentioned that the *Feigenbaum & Dafalias model* is strictly speaking only thermodynamically consistent in the case of small deformations. Although a finite strain version of the model has

been published in Feigenbaum (2008), this model is based on the Zaremba-Jaumann derivative for the elastic response. As stated in Xiao et al. (2000); Bruhns et al. (1999), such a model cannot fulfill the second law of thermodynamics. However, this inconsistency can be eliminated in a relatively straightforward manner, and thus, it is not serious.

In the present paper, different existing distortional hardening models are critically analyzed: the Teodosiu model (see Hiwatashi et al. (1998); Haddadi et al. (2006)), the Levkovitch & Svendsen model (see Barthel et al. (2008); Noman et al. (2010)) and the Feigenbaum & Dafalias model (see Feigenbaum and Dafalias (2007, 2008)). For a better comparison, they are reformulated into the modern framework of hyperelastoplasticity (cf. Simo and Hughes (1998); Simo (1998)) and the same objective time derivative is applied to all evolution equations. Although the respective modifications are relatively simple, they are crucial for thermodynamical consistency at finite strains. Furthermore, since the final goal pursued by the authors is the modeling of large-scale forming processes of magnesium sheets, the yield functions have to be modified. For that purpose, a Barlat-type yield function is employed, cf. Cazacu and Barlat (2004). In contrast to the yield function according to Hill, it is based on a modified 2nd as well as on a modified 3rd invariant of the stress tensor. Therefore, two different evolving fourth-order tensors defining the material's anisotropy can be introduced which is precisely advocated in the present paper. Based on the aforementioned extensions, all three models are compared with respect to their predictive capabilities for magnesium sheets. Furthermore, thermodynamical consistency of the models is critically analyzed. It will be shown that only the extended Feigenbaum & Dafalias model can fulfill the second law of thermodynamics. However and as mentioned before, that model predicts a high curvature of the yield function in loading direction, while the opposite region of the yield function is rather flat. Since this effect seems not to be correct for the considered magnesium sheets (see Plunkett et al. (2006)), a novel constitutive model is presented. Its underlying structure is surprisingly simple and the model is thermodynamically consistent. Conceptually, distortional hardening is described by an Armstrong-Frederick-type approach (cf. Mosler (2010)).

The paper is organized as follows: Firstly, the fundamentals of finite strain plasticity are briefly summarized in Section 2. Particularly the implications of material modeling principles such as material frame indifference, material symmetry and thermodynamical consistency are concisely discussed. The comparison of the Teodosiu (Subsection 3.1), the Levkovitch & Svendsen (Subsection 3.2) and the Feigenbaum & Dafalias model (Subsection 3.3) is elaborated in Section 3. Within each of the Subsections 3.1, 3.2 and 3.3, the original model is presented first. The modifica-

tions necessary for the modeling of magnesium are subsequently addressed. Finally, a novel thermodynamically consistent distortional hardening model suitable for the numerical analysis of magnesium is advocated in Section 4. Its predictive capabilities are demonstrated by comparisons to experimentally measured data.

2. Finite strain plasticity theory in a nutshell

2.1. Fundamentals

Following standard notations in continuum mechanics, material points P are identified by their position vectors. While such vectors are denoted as $\boldsymbol{X}$ within the undeformed configuration Ω, the lowercase letter $\boldsymbol{x}$ signals the spatial counterpart in the deformed configuration $\boldsymbol{\varphi}(\Omega)$. With these vectors, the deformation mapping $\boldsymbol{\varphi}$ is introduced in standard manner, i.e., $\boldsymbol{\varphi} : \Omega \ni \boldsymbol{X} \rightarrow \boldsymbol{x} \in \boldsymbol{\varphi}(\Omega)$. It is locally approximated by the deformation gradient $\boldsymbol{F} := \mathrm{GRAD}\boldsymbol{\varphi} = \partial\boldsymbol{\varphi}/\partial\boldsymbol{X}$.

Since elastoplastic deformation processes are considered within the present paper, it is convenient to decompose $\boldsymbol{F}$ into an elastic part $\boldsymbol{F}^{\mathrm{e}}$ and a plastic part $\boldsymbol{F}^{\mathrm{p}}$. More explicitly and in line with Lee (1969), the multiplicative decomposition

$$\boldsymbol{F} = \boldsymbol{F}^{\mathrm{e}} \cdot \boldsymbol{F}^{\mathrm{p}}, \qquad \text{with} \qquad \det \boldsymbol{F}^{\mathrm{e}} > 0, \ \det \boldsymbol{F}^{\mathrm{p}} > 0 \tag{1}$$

is adopted for that purpose. Since constitutive models suitable for analyzing plastic deformation are usually based on evolution equations for the inelastic strains $\boldsymbol{F}^{\mathrm{p}}$, deformation rates are also required. Analogously to the standard spatial velocity gradient

$$\boldsymbol{l} := \dot{\boldsymbol{F}} \cdot \boldsymbol{F}^{-1} \tag{2}$$

the two additional velocity gradients

$$\boldsymbol{L}^{\mathrm{p}} := \dot{\boldsymbol{F}}^{\mathrm{p}} \cdot [\boldsymbol{F}^{\mathrm{p}}]^{-1}, \qquad \boldsymbol{l}^{\mathrm{e}} := \dot{\boldsymbol{F}}^{\mathrm{e}} \cdot [\boldsymbol{F}^{\mathrm{e}}]^{-1} \tag{3}$$

are thus defined. Here, the superposed dot represents the material time derivative.

Similarly to the kinematics (1), the constitutive response is also decomposed into an elastic part Ψ^{e} and a plastic part Ψ^{p}. To be more precise, the Helmholtz energy Ψ is additively split according to

$$\Psi = \Psi^{\mathrm{e}}(\boldsymbol{F}^{\mathrm{e}}) + \Psi^{\mathrm{p}}(\boldsymbol{\alpha}). \tag{4}$$

Here, the energy Ψ^{e} is due to elastic distortion of the underlying atomic lattice, whereas Ψ^{p} depending on the suitable set of internal strain-like variables $\boldsymbol{\alpha}$ is related

to plastic hardening. In the present paper, Ψ^{p} will cover classical isotropic and kinematic hardening as well as distortional hardening (distortion of the yield function). Application of the meanwhile standard Coleman & Noll procedure (see Coleman and Gurtin (1967)) yields the stress response

$$\boldsymbol{P} = \partial_{\boldsymbol{F}} \Psi \tag{5}$$

together with the reduced dissipation inequality

$$\mathcal{D} = \boldsymbol{\Sigma} : \boldsymbol{L}^{\mathrm{p}} + \boldsymbol{Q} \cdot \dot{\boldsymbol{\alpha}} \geq 0, \qquad \boldsymbol{Q} := -\partial_{\boldsymbol{\alpha}} \Psi. \tag{6}$$

Here, $\boldsymbol{P}$ is the first Piola-Kirchhoff stress tensor, $\boldsymbol{\Sigma} = 2\, \boldsymbol{C}^{\mathrm{e}} \cdot \partial_{\boldsymbol{C}^{\mathrm{e}}} \Psi$ is the Mandel stress tensor (with respect to the intermediate configuration) and $\boldsymbol{Q}$ is the stress-like internal variable energetically conjugate to $\boldsymbol{\alpha}$. In addition to the numerical advantages of hyperelastoplastic formulations such as the one defined by Eq. (4) (see Simo and Hughes (1998); Simo (1998)), the introduction of a stored energy is also required for proving thermodynamical consistency (e.g. the second law of thermodynamics). An equally important fact is that models not consistently derived from an energy potential such as hypoelastoplasticity approaches do usually not obey the second law of thermodynamics for elastic unloading, cf. Xiao et al. (2000); Bruhns et al. (1999). In summary, the choice of a framework for finite strain plasticity theory is not always only a matter of taste.

While for elastic unloading ($\boldsymbol{L}^{\mathrm{p}} = \boldsymbol{0}$ and $\dot{\boldsymbol{\alpha}} = \boldsymbol{0}$), the dissipation inequality (6) is evidently fulfilled, that is not automatically the case for elastoplastic processes. A thermodynamically consistent framework a priori guaranteeing Ineq. (6) is that of *generalized standard materials*, cf. Mandel (1971); Lemaitre (1985). This framework requires an additional response function: the so-called *plastic potential* g. With this potential g, the flow rule and the hardening rules are assumed to be

$$\boldsymbol{L}^{\mathrm{p}} = \lambda\, \partial_{\boldsymbol{\Sigma}} g \qquad \dot{\boldsymbol{\alpha}} = \lambda\, \partial_{\boldsymbol{Q}} g. \tag{7}$$

In Eq. (7), $\lambda \geq 0$ is the non-negative plastic multiplier. It can be seen in a straightforward manner that Ineq. (6) is always fulfilled, provided the plastic potential is convex (and non-negative for plastic loading).

To complete the model, the plastic multiplier $\lambda \geq 0$ has to be determined for elastoplastic loading. Usually, the space of admissible stresses $\mathbb{E}_{\boldsymbol{\Sigma}}$ is introduced for this reason. In line with the reduced dissipation inequality (6), this space is formulated in terms of $\boldsymbol{\Sigma}$ and $\boldsymbol{Q}$, i.e.,

$$\mathbb{E}_{\boldsymbol{\Sigma}} = \left\{ (\boldsymbol{\Sigma}, \boldsymbol{Q}) \in \mathbb{R}^{9+n} \;\middle|\; \phi(\boldsymbol{\Sigma}, \boldsymbol{Q}) \leq 0 \right\}. \tag{8}$$

Here, ϕ is the yield function which has to fulfill certain regularity conditions such as convexity. With the help of space (8), the loading and unloading conditions can be written in the classical Karush-Kuhn-Tucker form

$$\lambda\ \phi = 0, \qquad \lambda\ \dot{\phi} = 0. \tag{9}$$

and the plastic multiplier λ is computed from the consistency condition $\dot{\phi} = 0$.

Remark 1. *According to Eqs. (8) and (7), a description with respect to the intermediate configuration is chosen. Such a description is well known to automatically fulfill the principle of material frame indifference. Hence, arbitrary material symmetries can be modeled in a straightforward manner. That is certainly of utmost importance in the case of texture evolution. Although frequently seen in the literature, anisotropic yield functions in terms of Cauchy stresses cannot fulfill the principle of material frame indifference (except if evolving structural tensors are also introduced, cf. Xiao et al. (2000); Bruhns et al. (1999)).*

2.2. A prototype model for magnesium

A yield function suitable for the modeling of magnesium alloys (polycrystals) has to capture the stress differential effect, the material's symmetry (anisotropy) and, in line with the underlying atomic lattice structure of the material, it should only depend on the stress deviator. Such a function was presented in a series of papers by Barlat and co-workers, cf. Cazacu and Barlat (2004). In line with Mekonen et al. (2012), this model is rewritten in tensor notation here and re-formulated in terms of Mandel stresses automatically fulfilling the principle of material frame indifference. Considering isotropic hardening (the related stress-like internal variable is denoted as Q_{iso}) and in contrast to Cazacu and Barlat (2004); Mekonen et al. (2012) also kinematic hardening (the related stress-like internal variable is denoted as $\boldsymbol{Q}_{\mathrm{kin}}$), the yield function reads

$$\phi = J_2^{\frac{3}{2}} - J_3 - Q_0^3 - Q_{\mathrm{iso}}^3. \tag{10}$$

Here, Q_0 is the yield stress associated with the initial yield surface and J_2 and J_3 are modified second and third invariants of the effective stresses $\boldsymbol{\Sigma} - \boldsymbol{Q}_{\mathrm{kin}}$. They are defined as

$$J_2 := \frac{1}{2}\,\mathrm{tr}\left[\boldsymbol{\xi}_1 \cdot \boldsymbol{\xi}_1\right], \quad J_3 := \frac{1}{3}\mathrm{tr}\left[\boldsymbol{\xi}_2 \cdot \boldsymbol{\xi}_2 \cdot \boldsymbol{\xi}_2\right], \qquad \mathrm{tr}(\bullet) := (\bullet) : \mathbf{1} \tag{11}$$

with the linear transformations

$$\boldsymbol{\xi}_i := \mathbb{H}_i : (\boldsymbol{\Sigma} - \boldsymbol{Q}_{\mathrm{kin}}), \qquad i \in \{1; 2\}. \tag{12}$$

According to Eq. (12), the material's anisotropy is captured by the fourth-order tensors $\mathbb{H}_i$. Consequently, a distortion of the yield surface can be captured by suitable evolution equations of the type $\dot{\mathbb{H}}_i = \mathbb{F}(\lambda)$. Speaking from a physics point of view, such equations are related to the evolution of the underlying microstructure. In the present section, this effect is however not yet considered.

The model is completed by defining evolution equations and the Helmholtz energy. Concerning the latter, the isotropic neo-Hooke-type energy

$$\Psi^{\mathrm{e}}(\boldsymbol{C}^{\mathrm{e}}) = \frac{\Lambda}{4}\left(J^{\mathrm{e}2} - 1\right) - \left(\frac{\Lambda}{2} + \mu\right) \ln J^{\mathrm{e}} + \frac{\mu}{2}\left(\mathrm{tr}\boldsymbol{C}^{\mathrm{e}} - 3\right) \tag{13}$$

is adopted, since the elastic response of magnesium is not strongly anisotropic. In Eq. (13), Λ and μ represent the Lamé parameters and $J^{\mathrm{e}} := \det \boldsymbol{F}^{\mathrm{e}}$, cf. Ogden (1997). Regarding the part Ψ^{p} of the Helmholtz energy due to cold work, a decoupling of isotropic and kinematic hardening resulting in the additive split

$$\Psi^{\mathrm{p}}(\alpha_{\mathrm{iso}}, \boldsymbol{\alpha}_{\mathrm{kin}}) = \Psi^{\mathrm{p}}_{\mathrm{iso}}(\alpha_{\mathrm{iso}}) + \Psi^{\mathrm{p}}_{\mathrm{kin}}(\boldsymbol{\alpha}_{\mathrm{kin}}) \tag{14}$$

is assumed. Here, α_{iso} and $\boldsymbol{\alpha}_{\mathrm{kin}}$ are strain-like internal variables conjugate to $Q_{\mathrm{iso}} := -\partial_{\alpha_{\mathrm{iso}}}\Psi$ and $\boldsymbol{Q}_{\mathrm{kin}} := -\partial_{\boldsymbol{\alpha}_{\mathrm{kin}}}\Psi$, respectively. Furthermore and with focus on non-linear kinematic hardening of Armstrong-Frederick-type, $\Psi^{\mathrm{p}}_{\mathrm{kin}}$ is specified to

$$\Psi^{\mathrm{p}}_{\mathrm{kin}}(\boldsymbol{\alpha}_{\mathrm{kin}}) = \frac{1}{2}\, c_{\mathrm{kin}}\, \boldsymbol{\alpha}_{\mathrm{kin}} : \boldsymbol{\alpha}_{\mathrm{kin}} \tag{15}$$

where c_{kin} is the kinematic hardening modulus. Finally, the plastic potential

$$g = \phi + \frac{1}{2}\,\frac{b_{\mathrm{kin}}}{c_{\mathrm{kin}}}\, \boldsymbol{Q}_{\mathrm{kin}} : \boldsymbol{Q}_{\mathrm{kin}} \tag{16}$$

defining the flow rule and the evolution equations is adopted, see Eq. (7). The model parameter b_{kin} defines the saturation value of the back strain $\boldsymbol{\alpha}_{\mathrm{kin}}$. According to Eq. (16), an associative flow rule and an associative evolution equation for isotropic hardening are chosen, whereas kinematic hardening is governed by the differential equation

$$\dot{\boldsymbol{\alpha}}_{\mathrm{kin}} = \lambda\, \partial_{\boldsymbol{Q}_{\mathrm{kin}}} g = -\lambda\, \partial_{\boldsymbol{\Sigma}}\phi - \lambda\, b_{\mathrm{kin}}\, \boldsymbol{\alpha}_{\mathrm{kin}}. \tag{17}$$

Neglecting kinematic hardening, model parameters calibrated for the magnesium alloys AZ31 and ZE10 can be found in Mekonen et al. (2012).

Remark 2. *Since usually* $||\partial_{\boldsymbol{\Sigma}}\phi|| \neq 1$*, the flow direction* $\partial_{\boldsymbol{\Sigma}}\phi$ *in Eq. (17) is often replaced by its normalized counterpart* $\boldsymbol{N} := \partial_{\boldsymbol{\Sigma}}\phi/||\partial_{\boldsymbol{\Sigma}}\phi||$*. Combining this with* $\boldsymbol{Q}_{\text{kin}} = -c_{\text{kin}}\,\boldsymbol{\alpha}_{\text{kin}}$ *yields*

$$\dot{\boldsymbol{Q}}_{\text{kin}} = c_{\text{kin}} \left(\boldsymbol{N} - \frac{b_{\text{kin}}}{c_{\text{kin}}}\,\boldsymbol{Q}_{\text{kin}} \right) \lambda. \tag{18}$$

This representation of kinematic hardening will frequently be used in the present paper.

3. Modeling texture evolution by distortional hardening - a critical review of existing models and extensions necessary for magnesium alloys

The present section is concerned with a critical review of existing distortional hardening models. To be more precise, the Teodosiu model (see Hiwatashi et al. (1998); Haddadi et al. (2006)), the Levkovitch & Svendsen model (see Barthel et al. (2008); Noman et al. (2010)) and the Feigenbaum & Dafalias model (see Feigenbaum and Dafalias (2007, 2008)) are analyzed and compared. For a better comparison, they are reformulated into the modern framework of hyperelastoplasticity and the same consistent notation is used for the description of every model. In additional to the review, the extensions necessary for the modeling of texture evolution in magnesium alloys are also discussed. Finally, the fulfillment of fundamental principles of material modeling such as thermodynamical consistency is checked for the resulting novel models.

3.1. The Teodosiu model

3.1.1. Fundamentals

The fundamentals of the Teodosiu model are briefly given here. However and in contrast to the original works Hiwatashi et al. (1998); Peeters et al. (2002); Li et al. (2003); Haddadi et al. (2006), the notations as introduced within the previous section are used here.

The Teodosiu model is based on the modified Hill-type yield function

$$\phi = \bar{\Sigma}_{\text{e}} - Q_0 - Q_{\text{iso}} - f\|\mathbb{S}\| \tag{19}$$

with the equivalent relative stress

$$\bar{\Sigma}_{\text{e}} = \sqrt{(\text{dev}\boldsymbol{\Sigma} - \boldsymbol{Q}_{\text{kin}}) : \mathbb{H} : (\text{dev}\boldsymbol{\Sigma} - \boldsymbol{Q}_{\text{kin}})}. \tag{20}$$

where $\text{dev}\boldsymbol{\Sigma}$ is the deviator of $\boldsymbol{\Sigma}$, f is a model parameter and $\mathbb{H}$ and $\mathbb{S}$ are two fourth-order tensors. It bears emphasis that, in contrast to the original model,

Mandel stresses are considered here. The principle of material frame indifference is thereby fulfilled. The fourth-order tensor $\mathbb{H}$ in Eq. (20) defines the symmetry of the material which is kept constant in the original Teodosiu model ($\dot{\mathbb{H}} = \mathbf{0}$). The only non-standard term in the yield function (19) is the fourth-order tensor $\mathbb{S}$. As will be shown, this tensor captures, among others, the cross hardening effect (see Haddadi et al. (2006)).

Isotropic and kinematic hardening are governed by the classical Armstrong-Frederick evolution equations (compare to Eq. (18))

$$\dot{Q}_{\text{iso}} = c_{\text{iso}} \ (Q^{\infty}_{\text{iso}} - Q_{\text{iso}}) \ \lambda \tag{21}$$

and

$$\dot{\boldsymbol{Q}}_{\text{kin}} = c_{\text{kin}} \ (Q^{\infty}_{\text{kin}} \ \boldsymbol{N} - \boldsymbol{Q}_{\text{kin}}) \ \lambda, \qquad \boldsymbol{N} := \frac{\partial_{\boldsymbol{\Sigma}} \phi}{||\partial_{\boldsymbol{\Sigma}} \phi||}. \tag{22}$$

In line with the notation introduced in the previous section, c_{iso} and c_{kin} are the isotropic and the kinematic hardening moduli and Q^{∞}_{iso} and Q^{∞}_{kin} are the saturation limits associated with isotropic and kinematic hardening. The only, but nevertheless crucial, difference compared to standard non-linear kinematic hardening is that the saturation limit Q^{∞}_{kin} is not a constant model parameter, but depends on the fourth-order tensor $\mathbb{S}$. Before giving the explicit expression, the physical interpretation of $\mathbb{S}$ is briefly discussed.

Within the Teodosiu model, the strength due to dislocation structures is decomposed into a part associated with the currently active slip systems (denoted as $\mathbb{S}_{\text{D}}$) and the one related to latent slip systems (denoted as $\mathbb{S}_{\text{L}}$). For such parts, Teodosiu postulated the evolution equations

$$\dot{\mathbb{S}}_{\text{L}} = -c_{\text{SL}} \ \left(\frac{\|\mathbb{S}_{\text{L}}\|}{S^{\infty}} \right)^{n_{\text{L}}} \mathbb{S}_{\text{L}} \ \lambda \tag{23}$$

and

$$\dot{S}_{\text{D}} = c_{\text{SD}} \ [\tilde{g} \ (S^{\infty} - S_{\text{D}}) - h \ S_{\text{D}}] \ \lambda. \tag{24}$$

According to Eqs. (23) and (24), no evolution equation for the total tensor $\mathbb{S}$ is assumed. As stated in Wang et al. (2008), that leads to mathematical problems. To be more precise, the Teodosiu model is overdetermined from a mathematical point of view. However, this deficiency is not crucial, since it can be eliminated in a straightforward manner, cf. Wang et al. (2008). The respective modification has been considered in the final implementation. While c_{SL}, c_{SD}, n_{L} and S^{∞} are constant model parameters, $\tilde{g}$ and h are deformation-dependent. Without going into too much

detail, such functions are related to the effects of work hardening stagnation and resumption, cf. Haddadi et al. (2006). These effects, although important for some applications, are not the focus of the present paper. Therefore, they are not discussed here. The interested reader is referred to Remark 3.

Having defined the evolution of the fourth-order tensor $\mathbb{S}$, the saturation value $Q_{\mathrm{kin}}^{\infty}$ is postulated to be

$$Q_{\mathrm{kin}}^{\infty} = Q_{\mathrm{kin}}^{(0)} + (1-f)\sqrt{r\,\|\mathbb{S}\|^2 + (1-r)\,S_{\mathrm{D}}^2} \tag{25}$$

where r is a weighting factor and $Q_{\mathrm{kin}}^{(0)}$ is another model parameter. Accordingly and in sharp contrast to a conventional Armstrong-Frederick-type law, the saturation value is non-constant and implicitly depends on the loading path. Furthermore, Eq. (25) implies a strong coupling between kinematic and distortional hardening.

To understand the fundamentals of the model, a monotonic uniaxial loading test followed by orthogonal loading is considered. Assuming a well-annealed material ($\mathbb{S} = \mathbf{0}$), $\mathbb{S} = S_{\mathrm{D}}\boldsymbol{N}_1 \otimes \boldsymbol{N}_1$ during the first loading stage with $\boldsymbol{N}_1$ denoting the respective (constant) flow direction. Furthermore, $\mathbb{S}_{\mathrm{L}} = \mathbf{0}$. Altogether, that leads to a standard coupled isotropic/kinematic hardening response within a kinematic saturation limit of $Q_{\mathrm{kin}}^{\infty} = Q_{\mathrm{kin}}^{(0)} + (1-f)\,||\mathbb{S}||$ (since $||\mathbb{S}|| = S_{\mathrm{D}}$ during the first loading stage). When the loading path is subsequently changed, indicated by $\boldsymbol{N}_2$, the new initial conditions are $S_{\mathrm{D}} = \boldsymbol{N}_2 : \mathbb{S} : \boldsymbol{N}_2$ and $\mathbb{S}_{\mathrm{L}} = \mathbb{S} - S_{\mathrm{D}}\boldsymbol{N}_2 \otimes \boldsymbol{N}_2$. Consequently, the part of $\mathbb{S}$ which was related to the currently active dislocations during the first loading stage, now corresponds to latent slip systems. While isotropic hardening is not affected by this flip, since it depends only on the equivalent plastic strain α_{iso} and the norm of $\mathbb{S}$, it leads to the different saturation value $Q_{\mathrm{kin}}^{\infty} = Q_{\mathrm{kin}}^{(0)} + (1-f)\,\sqrt{r}\,||\mathbb{S}||$ for kinematic hardening. Thus, if $r > 1$, the new saturation value is higher, resulting in a cross hardening effect.

A careful analysis reveals that isotropic, kinematic and distortional hardening are strongly coupled within the Teodosiu model. For this reason, a precise interpretation of the model and its interactions is not straightforward, although the underlying idea can be relatively well understood by considering the aforementioned mechanical experiment (orthogonal loading). Furthermore and equally important, the cross hardening effect is only taken into account through kinematic hardening. That can be seen as follows: Isotropic hardening cannot contribute to cross hardening. Furthermore, $||\mathbb{S}||$ is also constant, if the loading path changes. Therefore, the only possibility to describe cross hardening is through the back stress, see Eq. (19). This is indeed the case, since the saturation value $Q_{\mathrm{kin}}^{\infty}$ is sensitive with respect to a change of the loading path as discussed in the previous paragraph. However, that is the only

consideration of cross hardening within the model. In particular, a distortion of the yield function is not accounted for. In summary, the main motivation for the Teodosiu model seems to be the precise description of work hardening stagnation, softening and resumption.

Remark 3. *For the sake of completeness, the functions $\tilde{g}$ and h governing the evolution of $\mathbb{S}$ due to currently active dislocations are briefly discussed here, cf. Eq. (24). The latter is given by*

$$h = \frac{1}{2}\left(1 - \frac{\boldsymbol{Q}_{\text{kin}} : \boldsymbol{N}}{Q^{\infty}_{\text{kin}}\ (dev\boldsymbol{\Sigma} - \boldsymbol{Q}_{\text{kin}}) : \boldsymbol{N}}\ \bar{\Sigma}_{\text{e}}\right). \tag{26}$$

Accordingly, Eq. (26) defines an interaction between kinematic hardening and the fourth-order tensor $\mathbb{S}$ and leads to a small decrease in S_{D} (the rate) at the beginning of a reversed deformation path, cf. Haddadi et al. (2006).

In contrast to h, the function $\tilde{g}$ depends on the so-called polarity tensor $\boldsymbol{P}$ *introduced by the Armstrong-Frederick-rule*

$$\dot{\boldsymbol{P}} = c_P\,(\boldsymbol{N} - \boldsymbol{P})\ \lambda \tag{27}$$

Here, c_P is a model parameter. In the sense of physics, $\boldsymbol{P}$ grows into the direction of the current plastic flow direction. However, $\boldsymbol{P}$ does not change its direction spontaneously which is implemented by the memory term $\boldsymbol{P}\,\lambda$ in Eq. (27). Loading path changes can be identified by the projection

$$P_{\text{D}} = \boldsymbol{P} : \boldsymbol{N}. \tag{28}$$

With this projection, the function $\tilde{g}$ in Eq. (24) is defined as

$$\tilde{g} = \begin{cases} 1 - \frac{c_P}{c_{\text{SD}}+c_P}\left|\frac{S_{\text{D}}}{S^{\infty}} - P_{\text{D}}\right| & \text{if } P_{\text{D}} \geq 0 \\ (1+P_{\text{D}})^{n_P}\left(1 - \frac{c_P}{c_{\text{SD}}+c_P}\frac{S_{\text{D}}}{S^{\infty}}\right) & \text{otherwise} \end{cases} \tag{29}$$

where n_P is another model parameter. As explained in Haddadi et al. (2006), the continuous function $\tilde{g}$ has been designed to capture work hardening stagnation and resumption.

3.1.2. Extensions of the Teodosiu model for magnesium alloys

By combining Eqs. (10) and (19), the Teodosiu model can be incorporated into the Barlat-type yield function (Cazacu and Barlat, 2004), i.e.

$$\phi = J_2^{\frac{3}{2}} - J_3 - Q_0^3 - Q_{\text{iso}}^3 - f\,\|\mathbb{S}\|. \tag{30}$$

Certainly, two different fourth-order tensors $\mathbb{S}_1$ and $\mathbb{S}_2$ could also have been introduced resulting in

$$\phi = J_2^{\frac{3}{2}} - J_3 - Q_0^3 - Q_{\text{iso}}^3 - f_1 \left\|\mathbb{S}_1\right\| - f_2 \left\|\mathbb{S}_2\right\|. \tag{31}$$

However, since $\mathbb{S}$ affects only isotropic and kinematic hardening, both formulations are essentially equivalent. Due to computational efficiency, only one tensor $\mathbb{S}$ is thus chosen here. In line with Wang et al. (2008), this tensor is assumed to be governed by the evolution equation

$$\dot{\mathbb{S}} = \underbrace{\lambda\, \tilde{g}\, c_{\text{SD}}\, S^{\infty}\, \boldsymbol{N} \otimes \boldsymbol{N} - \lambda\, (\tilde{g} + h)\, c_{\text{SD}}\, S_{\text{D}}\, \boldsymbol{N} \otimes \boldsymbol{N}}_{= \dot{S}_{\text{D}}\, \boldsymbol{N} \otimes \boldsymbol{N},\ \text{see Eq. (24)}} \underbrace{- \lambda\, c_{\text{SL}} \left\{ \frac{\left\|\mathbb{S}_{\text{L}}\right\|}{S^{\infty}} \right\}^{n_{\text{L}}} \mathbb{S}_{\text{L}}}_{= \dot{\mathbb{S}}_{\text{L}},\ \text{see Eq. (23))}}. \tag{32}$$

Although formally identical to Eq. (24) and Eq. (23), the modified Teodosiu-type evolution equation (32) solves the mathematical inconsistencies of the original model, cf. Wang et al. (2008). While the function $\tilde{g}$ in Eq. (32) has not to be changed, that is not the case for h. This function reads

$$h = \frac{1}{2} \left(1 - \frac{\boldsymbol{Q}_{\text{kin}} : \boldsymbol{N}}{Q_{\text{kin}}^{\infty}\, (\text{dev}\boldsymbol{\Sigma} - \boldsymbol{Q}_{\text{kin}}) : \boldsymbol{N}} \bar{\Sigma}_{\text{e}} \right), \tag{33}$$

and hence, it depends through $\bar{\Sigma}_{\text{e}}$ on the shape of the yield function, see Eqs. (19) and (20). Inspired by Eq. (30), the equivalent stress measure $\bar{\Sigma}_{\text{e}}$ is chosen as

$$\bar{\Sigma}_{\text{e}} = \left| \left(J_2^{\frac{3}{2}} - J_3 \right)^{\frac{1}{3}} \right|. \tag{34}$$

The remaining equations do not have to be modified, i.e., isotropic and kinematic hardening are still governed by Eqs. (21) and (22) and an associative flow rule is adopted.

3.1.3. Thermodynamical consistency

In the present section, thermodynamical consistency of the resulting model is analyzed. Since thermodynamical aspects have not been considered in the original Teodosiu model, some additional assumptions are required. Strictly speaking, without specifying an energy, one can neither prove nor disprove thermodynamical consistency.

To analyze thermodynamical consistency, the additional assumption

$$\Psi^{\text{p}} = \Psi^{\text{p}}_{\text{iso}}(\alpha_{\text{iso}}) + \Psi^{\text{p}}_{\text{kin}}(\boldsymbol{\alpha}_{\text{kin}}) + \Psi^{\text{p}}_{\text{dist}}(\mathbb{E}), \qquad \mathbb{S} := -\partial_{\mathbb{E}} \Psi \tag{35}$$

is made, i.e., the energy due to cold work is decomposed into isotropic, kinematic and distortional hardening (or cross hardening). While the exponential function

$$\Psi^{\mathrm{p}}_{\mathrm{iso}}(\alpha_{\mathrm{iso}}) = Q^{\infty}_{\mathrm{iso}} \left(\alpha_{\mathrm{iso}} + \frac{1}{c_{\mathrm{iso}}} \exp\left[-c_{\mathrm{iso}}\ \alpha_{\mathrm{iso}}\right] \right) \tag{36}$$

is assumed for isotropic hardening, quadratic functions are chosen for kinematic and cross hardening, i.e.

$$\Psi^{\mathrm{p}}_{\mathrm{kin}} := \frac{1}{2}\ \tilde{c}_{\mathrm{kin}}\ \boldsymbol{\alpha}_{\mathrm{kin}} : \boldsymbol{\alpha}_{\mathrm{kin}}, \quad \Psi^{\mathrm{p}}_{\mathrm{dist}} := \frac{1}{2}\ c_{\mathrm{dist}}\ \mathbb{E} :: \mathbb{E}. \tag{37}$$

Here $\mathbb{E}$ is an internal variable conjugate to $\mathbb{S}$. Since the closed-form solution of Eq. (21) yields an exponential hardening response $Q(\alpha_{\mathrm{iso}})$, Eq. (36) is equivalent to the assumption within the original Teodosiu model. The quadratic functions (37) are motivated from the analogy between Eq. (22) and the classical Armstrong-Frederick model (compare Eq. (37) to Eq. (15) and Eq. (22) to Eq. (17)).

With such assumptions, the reduced dissipation inequality (6) is obtained as

$$\mathcal{D} = \boldsymbol{\Sigma} : \boldsymbol{L}^{\mathrm{p}} + Q_{\mathrm{iso}}\ \dot{\alpha}_{\mathrm{iso}} + \boldsymbol{Q}_{\mathrm{kin}} : \dot{\boldsymbol{\alpha}}_{\mathrm{kin}} + \mathbb{S} :: \dot{\mathbb{E}} \geq 0. \tag{38}$$

Implicitly, the existence of a hyperelastic response has been assumed in Ineq. (38), see Eq. (4). Inserting the evolution equations (32), (22), together with the associative flow rule $\boldsymbol{L}^{\mathrm{p}} = \lambda\ \partial_{\boldsymbol{\Sigma}}\phi$ and the associative hardening rule

$$\dot{\alpha}_{\mathrm{iso}} = \lambda\ \frac{\partial \phi}{\partial Q_{\mathrm{iso}}} = -3\ \lambda\ Q^2_{\mathrm{iso}} \tag{39}$$

into the reduced dissipation inequality (38), yields after a lengthy, but nevertheless straightforward, transformation

$$\begin{aligned}
\mathcal{D} \ = \ & 3\ \lambda\ Q_0^3 + 3\ \lambda\ f\ \|\mathbb{S}\| \\
& + \lambda \left(\left\| \frac{\partial \phi}{\partial \boldsymbol{\Sigma}} \right\| - \frac{c_{\mathrm{kin}}}{\tilde{c}_{\mathrm{kin}}} Q^{\infty}_{\mathrm{kin}} \right) \boldsymbol{Q}_{\mathrm{kin}} : \boldsymbol{N} + \lambda\ \frac{c_{\mathrm{kin}}}{\tilde{c}_{\mathrm{kin}}} \boldsymbol{Q}_{\mathrm{kin}} : \boldsymbol{Q}_{\mathrm{kin}} \\
& + \lambda \left(\frac{c_{\mathrm{SD}}}{c_{\mathrm{dist}}} (\tilde{g} + h)\ \boldsymbol{N} : \mathbb{S} : \boldsymbol{N} - \frac{c_{\mathrm{SD}}\ S^{\infty}}{c_{\mathrm{dist}}}\ \tilde{g} \right) \mathbb{S} :: (\boldsymbol{N} \otimes \boldsymbol{N}) \\
& + \lambda\ \frac{c_{\mathrm{SL}}}{c_{\mathrm{dist}}} \left\{ \frac{\| \mathbb{S} - (\boldsymbol{N} : \mathbb{S} : \boldsymbol{N})\ \boldsymbol{N} \otimes \boldsymbol{N} \|}{S^{\infty}} \right\}^{n_{\mathrm{L}}} \mathbb{S} \\
& :: \left[\mathbb{S} - (\boldsymbol{N} : \mathbb{S} : \boldsymbol{N})\ \boldsymbol{N} \otimes \boldsymbol{N} \right] \geq 0.
\end{aligned} \tag{40}$$

Here, the positive homogeneity of degree three of the yield function with respect to isotropic, distortional hardening and the relative stresses has been used (for each

of the aforementioned variables independently). The terms $3\ \lambda\ Q_0^3$, $3\ \lambda\ f\ \|\mathbb{S}\|$ and $\lambda\ c_{\mathrm{kin}}/\tilde{c}_{\mathrm{kin}}\ \boldsymbol{Q}_{\mathrm{kin}} : \boldsymbol{Q}_{\mathrm{kin}}$ are clearly non-negative. Accordingly, sufficient conditions for thermodynamical consistency are given by

$$\lambda \left(\left\| \frac{\partial \phi}{\partial \boldsymbol{\Sigma}} \right\| - \frac{c_{\mathrm{kin}}}{\tilde{c}_{\mathrm{kin}}} Q_{\mathrm{kin}}^{\infty} \right) \boldsymbol{Q}_{\mathrm{kin}} : \boldsymbol{N} \geq 0 \tag{41}$$

and

$$\lambda \left(\frac{c_{\mathrm{SD}}}{c_{\mathrm{dist}}} \left(\tilde{g} + h \right) \boldsymbol{N} : \mathbb{S} : \boldsymbol{N} - \frac{c_{\mathrm{SD}}\, S^{\infty}}{c_{\mathrm{dist}}}\, \tilde{g} \right) \mathbb{S} :: (\boldsymbol{N} \otimes \boldsymbol{N}) \tag{42}$$

$$+\lambda\, \frac{c_{\mathrm{SL}}}{c_{\mathrm{dist}}} \left\{ \frac{\| \mathbb{S} - (\boldsymbol{N} : \mathbb{S} : \boldsymbol{N})\ \boldsymbol{N} \otimes \boldsymbol{N} \|}{S^{\infty}} \right\}^{n_{\mathrm{L}}} \mathbb{S} \tag{43}$$

$$:: \left[\mathbb{S} - (\boldsymbol{N} : \mathbb{S} : \boldsymbol{N})\ \boldsymbol{N} \otimes \boldsymbol{N} \right] \geq 0. \tag{44}$$

Such inequalities are evidently highly non-linear and thus, cannot be enforced in a straightforward manner. Unfortunately, without enforcing them, the dissipation inequality is usually not fulfilled. That could be confirmed by several numerical simulations.

3.2. The Levkovitch & Svendsen model

3.2.1. Fundamentals

The fundamentals of the Levkovitch & Svendsen model are concisely reviewed here. Further details can be found in Noman et al. (2010).

Neglecting distortional hardening, the Levkovitch & Svendsen model represents a special case of the Teodosiu model presented in the previous section. For instance, the yield function is obtained by setting the model parameter f in Eq. (19) to zero resulting in

$$\phi = \bar{\Sigma}_{\mathrm{e}} - Q_0 - Q_{\mathrm{iso}} \tag{45}$$

with

$$\bar{\Sigma}_{\mathrm{e}} = \sqrt{(\mathrm{dev}\boldsymbol{\Sigma} - \boldsymbol{Q}_{\mathrm{kin}}) : \mathbb{H} : (\mathrm{dev}\boldsymbol{\Sigma} - \boldsymbol{Q}_{\mathrm{kin}})}. \tag{46}$$

Furthermore, isotropic hardening is again defined by

$$\dot{Q}_{\mathrm{iso}} = c_{\mathrm{iso}} (Q_{\mathrm{iso}}^{\infty} - Q_{\mathrm{iso}})\ \lambda \tag{47}$$

whereas kinematic hardening is still governed by the evolution equation

$$\dot{\boldsymbol{Q}}_{\mathrm{kin}} = c_{\mathrm{kin}} (Q_{\mathrm{kin}}^{\infty}\ \boldsymbol{N} - \boldsymbol{Q}_{\mathrm{kin}})\ \lambda. \tag{48}$$

In contrast to the Teodosiu model, the material parameters c_{kin} and $Q_{\mathrm{kin}}^{\infty}$ in Eq. (48) are now constant, i.e., standard Armstrong-Frederick-type evolution equations are used (or Voce rule in the case of isotropic hardening).

Again in line with the Teodosiu model, the effects due to currently active dislocations (denoted as dynamic part in the Levkovitch & Svendsen model; indicated by the subscript D) and latent slip systems (denoted as latent part in the Levkovitch & Svendsen model; indicated by the subscript L) are described by a fourth-order tensor $\mathbb{A}$. Its evolution is assumed to be

$$\dot{\mathbb{A}} = c_{\mathrm{D}} \ \left(s_{\mathrm{D}} \ \boldsymbol{N} \otimes \boldsymbol{N} - \mathbb{A}_{\mathrm{D}}\right) \ \lambda + c_{\mathrm{L}} \ \left[s_{\mathrm{L}} \ \left(\mathbb{I}_{\mathrm{dev}} - \boldsymbol{N} \otimes \boldsymbol{N}\right) - \mathbb{A}_{\mathrm{L}}\right] \ \lambda. \tag{49}$$

where $\mathbb{I}_{\mathrm{dev}}$ is the fourth-order deviatoric projection tensor ($\mathrm{dev}\boldsymbol{A} = \mathbb{I}_{\mathrm{dev}} : \boldsymbol{A}$, $\forall \boldsymbol{A}$). Accordingly, the first term governing the dynamic part is of Armstrong-Frederick-type. The similarity to the Teodosiu model becomes evident, if the functions $\tilde{g}$ and h in Eq. (32) are assumed to be constant and uniaxial tension is considered. In this case, only the part due to the currently active slip systems evolves yielding an evolution equation of the form

$$\dot{\mathbb{S}} = \lambda \ a \ \boldsymbol{N} \otimes \boldsymbol{N} - \lambda \ b \ \mathbb{S} \tag{50}$$

for the Teodosiu model. By comparing Eq. (50) to the first term in Eq. (49), it can be clearly seen that the dynamic part in the Levkovitch & Svendsen model is a special case of the Teodosiu model. In contrast to Haddadi et al. (2006), the same evolution equation is also used for the latent part within the Levkovitch & Svendsen model, see Eq. (49).

So far, the Levkovitch & Svendsen model can be interpreted as a special case of the Teodosiu model in which hardening stagnation, softening and resumption have been excluded (the functions $\tilde{g}$ and h are constant model parameters). However, the crucial difference is that the fourth-order tensor $\mathbb{A}$ directly affects the shape of the yield function. This idea goes back to Baltov and Sawczuk (1965) and is implemented within the Levkovitch & Svendsen model by setting

$$\dot{\mathbb{H}} = \dot{\mathbb{A}}. \tag{51}$$

As a consequence of Eq. (51), the shape of the yield surface changes during deformation. That allows inclusion of the cross hardening effect in a consistent manner. Another important feature of the Levkovitch & Svendsen model is that isotropic, kinematic and distortional hardening are uncoupled (the evolution equations). Hereby, the physical interpretation of the equations becomes less complicated.

3.2.2. Extensions of the Levkovitch & Svendsen model for magnesium alloys

To model magnesium, the Hill yield function defined by Eqs. (45) and (46) is again replaced by the one proposed by Barlat and co-workers (Cazacu and Barlat, 2004), i.e.

$$\phi = J_2^{\frac{3}{2}} - J_3 - Q_0^3 - Q_{\text{iso}}^3. \tag{52}$$

According to Eqs. (10) and (11), the material's symmetry is captured within the Barlat-type yield function by the two fourth-order transformation tensors $\mathbb{H}_i$ ($J_2 = J_2(\mathbb{H}_1)$ and $J_3 = J_3(\mathbb{H}_2)$). Therefore, it is reasonable to introduce two independent evolution equations of the type (49). Consequently,

$$\dot{\mathbb{H}}_i = \lambda\, c_{\text{D}i}\, (s_{\text{D}i}\, \boldsymbol{N} \otimes \boldsymbol{N} - \mathbb{H}_{\text{D}i}) + \lambda\, c_{\text{L}i}\, [s_{\text{L}i}\, (\mathbb{I}_{\text{dev}} - \boldsymbol{N} \otimes \boldsymbol{N}) - \mathbb{H}_{\text{L}i}] \quad i \in \{1;2\} \tag{53}$$

is chosen.

Eqs. (52) and (53) are the only modifications required to adapt the Levkovitch & Svendsen model to magnesium. Isotropic and kinematic hardening are assumed to still be governed by Eqs. (47) and (48).

3.2.3. Thermodynamical consistency

Analogous to the Teodosiu model, thermodynamical aspects have not been considered in the original Levkovitch & Svendsen model. In particular, no Helmholtz energy was introduced. However an energy is required in order to analyze the second law of thermodynamics. For this reason, some additional assumptions are required.

The first assumption is the existence of an Helmholtz energy Ψ which is additively decomposed into Ψ^{e} and Ψ^{p}. While the neo-Hooke model (13) is adopted for Ψ^{e}, Ψ^{p} is additively split into the different hardening mechanisms, see Eq. (35). This split agrees with an uncoupling of the hardening mechanisms as considered within the original Levkovitch & Svendsen model. Assuming further that the hardening mechanisms governing the tensors $\mathbb{H}_1$ and $\mathbb{H}_2$ are also uncoupled, this eventually leads to

$$\Psi^{\text{p}}_{\text{dist}} = \Psi^{\text{p}}_{\text{dist1}} + \Psi^{\text{p}}_{\text{dist2}}, \quad \Psi^{\text{p}}_{\text{dist}i} := \frac{1}{2}\, c_{\text{dist}i}\, \mathbb{E}_i :: \mathbb{E}_i, \quad \mathbb{H}_i := -\partial_{\mathbb{E}_i} \Psi^{\text{p}} \tag{54}$$

Choosing again the exponential function (36) and the associative evolution equation (39) for isotropic hardening, the quadratic energy $(37)_1$ for kinematic hardening, together with the associative flow rule $\boldsymbol{L}^{\text{p}} = \lambda\, \partial_{\boldsymbol{\Sigma}} \phi$, the reduced dissipation inequality

$$\mathcal{D} = \boldsymbol{\Sigma} : \boldsymbol{L}^{\text{p}} + Q_{\text{iso}}\, \dot{\alpha}_{\text{iso}} + \boldsymbol{Q}_{\text{kin}} : \dot{\boldsymbol{\alpha}}_{\text{kin}} + \mathbb{H}_1 :: \dot{\mathbb{E}}_1 + \mathbb{H}_2 :: \dot{\mathbb{E}}_2 \geq 0 \tag{55}$$

can be rewritten as

$$\begin{aligned}\mathcal{D} \;=\; & 3\,\lambda\,Q_0^3 + \lambda\,\frac{c_{\mathrm{kin}}}{\tilde{c}_{\mathrm{kin}}}\,\boldsymbol{Q}_{\mathrm{kin}} : \boldsymbol{Q}_{\mathrm{kin}} + \lambda\,\frac{c_{\mathrm{L}i}}{c_{\mathrm{dist}i}}\mathbb{H}_i :: \mathbb{H}_i \\ & + \lambda\left(1 - \frac{c_{\mathrm{kin}}\,Q_{\mathrm{kin}}^{\infty}}{\tilde{c}_{\mathrm{kin}}\,||\partial_{\boldsymbol{\Sigma}}\phi||}\right)\,\boldsymbol{Q}_{\mathrm{kin}} : \partial_{\boldsymbol{\Sigma}}\phi \\ & - \lambda\,\frac{c_{\mathrm{L}i}\;s_{\mathrm{L}i}}{c_{\mathrm{dis}i}}\,\mathbb{H}_i :: \mathbb{I}_{\mathrm{dev}} \\ & - \lambda\,\frac{\left[c_{\mathrm{D}i}\,s_{\mathrm{D}i} - c_{\mathrm{L}i}\,s_{\mathrm{L}i} + (c_{\mathrm{L}i} - s_{\mathrm{L}i})\,\boldsymbol{N} : \mathbb{H}_i : \boldsymbol{N}\right]}{c_{\mathrm{dis}i}}\mathbb{H}_i :: (\boldsymbol{N}\otimes\boldsymbol{N}) \geq 0. \quad (56)\end{aligned}$$

Again, the positive homogeneity of degree three of the yield function with respect to isotropic, distortional hardening and the relative stresses has been used (for each of the aforementioned variables independently). In Eq. (56), a summation over i from one to two has to be carried out. Although the first line in Ineq. (56) is non-negative, a resulting overall non-negative dissipation can usually not be guaranteed. That was also confirmed by several numerical simulations. Furthermore, since the inequality is highly non-linear, it cannot be enforced in a straightforward manner during the calibration of the model parameters either.

3.3. The Feigenbaum & Dafalias model

3.3.1. Fundamentals

Finally, the fundamentals of the Feigenbaum & Dafalias model are briefly discussed. However and in contrast to the original works Feigenbaum and Dafalias (2007, 2008); Plesek et al. (2010), a finite strain description in terms of Mandel stresses is considered here in order to fulfill the principle of material frame indifference.

In line with the Teodosiu and the Levkovitch & Svendsen model, a Hill-type yield function represents the starting point. However, Feigenbaum & Dafalias considered the slightly different version

$$\phi = \bar{\Sigma}_{\mathrm{e}}^2 - Q_{\mathrm{iso}}^2, \quad (57)$$

with

$$\bar{\Sigma}_{\mathrm{e}} = \sqrt{(\mathrm{dev}\boldsymbol{\Sigma} - \boldsymbol{Q}_{\mathrm{kin}}) : \mathbb{H} : (\mathrm{dev}\boldsymbol{\Sigma} - \boldsymbol{Q}_{\mathrm{kin}})}. \quad (58)$$

Accordingly, the first term of the yield function is now positively homogeneous of degree two with respect to the relative stresses $\mathrm{dev}\boldsymbol{\Sigma} - \boldsymbol{Q}_{\mathrm{kin}}$, whereas it is positively homogeneous of degree one within the Teodosiu and the Levkovitch & Svendsen model.

Concerning isotropic and kinematic hardening, the Feigenbaum & Dafalias model is also based on Armstrong-Frederick-type evolution equations (or Voce rule). To be more precise the slightly modified equations

$$\dot{Q}_{\mathrm{iso}} = \lambda\, \kappa_1\, Q_{\mathrm{iso}}\, (1 - \kappa_2\, Q_{\mathrm{iso}}), \tag{59}$$

and

$$\dot{\boldsymbol{Q}}_{\mathrm{kin}} = \lambda\, ||\partial_{\boldsymbol{\Sigma}}\phi||\, a_1\, (\boldsymbol{N} - a_2\, \boldsymbol{Q}_{\mathrm{kin}}) \tag{60}$$

are employed where κ_1, κ_2, a_1 and a_2 are model parameters.

So far, all models show strong similarities. However, the distortion of the yield function is captured differently in Feigenbaum and Dafalias (2007, 2008); Plesek et al. (2010). To be more precise, the major goal pursued in Feigenbaum and Dafalias (2007) was to capture the higher curvature of the yield surface in loading direction and the respective flattening in the orthogonal direction. This effect is modeled through the projection of the effective current loading direction

$$\boldsymbol{N}_{\mathrm{r}} = \frac{\mathrm{dev}\boldsymbol{\Sigma} - \boldsymbol{Q}_{\mathrm{kin}}}{||\mathrm{dev}\boldsymbol{\Sigma} - \boldsymbol{Q}_{\mathrm{kin}}||} \tag{61}$$

onto the previous loading direction represented by the back stress. This projection shows some similarities to Eq. (28) within the Teodosiu model. Using the aforementioned projection, the fourth-order tensor $\mathbb{H}$ defining the shape of the yield functions is assumed as

$$\mathbb{H} = \mathbb{H}_0 + (\boldsymbol{N}_{\mathrm{r}} : \boldsymbol{Q}_{\mathrm{kin}})\mathbb{A} \tag{62}$$

where the fourth-order tensor $\mathbb{A}$ is introduced according to

$$\dot{\mathbb{A}} = -\lambda\, A_1\, ||\mathrm{dev}\boldsymbol{\Sigma} - \boldsymbol{Q}_{\mathrm{kin}}||^2 \left[(\boldsymbol{N}_{\mathrm{r}} : \boldsymbol{Q}_{\mathrm{kin}})\, \boldsymbol{N}_{\mathrm{r}} \otimes \boldsymbol{N}_{\mathrm{r}} + \frac{3}{2}\, A_2\, \mathbb{A}\right]. \tag{63}$$

Here, A_1 and A_2 are model parameters.

In order to understand the model, the aforementioned projection which describes the curvature difference in the loading, the opposite direction is switched off first by setting $\boldsymbol{N}_{\mathrm{r}} : \boldsymbol{Q}_{\mathrm{kin}} = 1$. In this case, Eqs. (62) and (63) can be simplified to

$$\dot{\mathbb{H}} = -\lambda\, A_1 \left[(\mathrm{dev}\boldsymbol{\Sigma} - \boldsymbol{Q}_{\mathrm{kin}}) \otimes (\mathrm{dev}\boldsymbol{\Sigma} - \boldsymbol{Q}_{\mathrm{kin}}) + \frac{3}{2}\, A_2\, ||\mathrm{dev}\boldsymbol{\Sigma} - \boldsymbol{Q}_{\mathrm{kin}}||^2\, \mathbb{A}\right]. \tag{64}$$

According to Eq. (64) and in line with the Levkovitch & Svendsen model (see Eq. (49)) and the Teodosiu model (see Eq. (32)), distortional hardening is again

modeled by an Armstrong-Frederick-type evolution equation. The only slight difference is that the flow direction $\boldsymbol{N}$ is replaced by the "radial" direction $\boldsymbol{N}_{\mathrm{r}}$ in Eq. (64). However, that does not lead to significant differences. Furthermore, all effects are incorporated into only one evolution equation in the Feigenbaum & Dafalias model. By way of contrast, a decomposition into dynamic and latent parts is considered within the Teodosiu as well as within the Levkovitch & Svendsen model.

Having discussed the special situation $\boldsymbol{N}_{\mathrm{r}} : \boldsymbol{Q}_{\mathrm{kin}} = 1$, focus is now on the general case. Conceptually, distortional hardening is still modeled by an Armstrong-Frederick-type evolution equation then. However, according to the factor $\boldsymbol{N}_{\mathrm{r}} : \boldsymbol{Q}_{\mathrm{kin}}$ the effective material parameters of this evolution equation can change - even their signs. Precisely this yields a higher curvature of the yield function in loading direction and a flattening in the opposite direction.

In summary, the only major difference between the Feigenbaum & Dafalias model and the Levkovitch & Svendsen model is the projection factor $\boldsymbol{N}_{\mathrm{r}} : \boldsymbol{Q}_{\mathrm{kin}}$. However, that factor does have an important effect on the evolution of the yield function. It is realized by a coupling between kinematic and distortional hardening through which the overall model becomes more complex.

3.3.2. Extensions of the Feigenbaum & Dafalias model model for magnesium alloys

Based on the similarities between the original Feigenbaum & Dafalias model and the original Levkovitch & Svendsen model, the extensions necessary for the description of magnesium are similar as well. Conceptually, the only significant difference is related to distortional hardening. In this connection, the two fourth-order tensors (53) governing the evolution of the original Barlat-type yield function (52) are assumed to be

$$\mathbb{H}_i = \mathbb{H}_{0i} + (\boldsymbol{N}_{\mathrm{r}} : \boldsymbol{Q}_{\mathrm{kin}})\, \mathbb{A}_i \qquad i \in \{1;2\}. \tag{65}$$

Both fourth-order tensors $\mathbb{A}_i$ are independently governed by equation (63), i.e.,

$$\dot{\mathbb{A}}_i = -\lambda\, A_{1i}\, ||\mathrm{dev}\boldsymbol{\Sigma} - \boldsymbol{Q}_{\mathrm{kin}}||^2 \left[(\boldsymbol{N}_{\mathrm{r}} : \boldsymbol{Q}_{\mathrm{kin}})\, \boldsymbol{N}_{\mathrm{r}} \otimes \boldsymbol{N}_{\mathrm{r}} + \frac{3}{2}\, A_{2i}\, \mathbb{A}_i \right]. \tag{66}$$

3.3.3. Thermodynamical consistency

The Feigenbaum & Dafalias model is the only one of the distortional hardening approaches which has been derived from thermodynamical principles. Therefore, its original form fulfills the dissipation inequality within a geometrically linearized setting. However, here the more general case is considered. To be more precise, the extended model with the yield function as proposed in Cazacu and Barlat (2004) and a finite strain hyperelastoplasticity framework is adopted (see Section 2).

Following Subsection 3.2.3, the Helmholtz energy is additively decomposed according to

$$\Psi = \Psi^{\mathrm{e}} + \Psi^{\mathrm{p}}_{\mathrm{iso}}(\alpha_{\mathrm{iso}}) + \Psi^{\mathrm{p}}_{\mathrm{kin}}(\boldsymbol{\alpha}_{\mathrm{kin}}) + \Psi^{\mathrm{p}}_{\mathrm{dist1}}(\mathbb{E}_1) + \Psi^{\mathrm{p}}_{\mathrm{dist2}}(\mathbb{E}_2) \tag{67}$$

with

$$\Psi^{\mathrm{e}} = \text{Eq. (13)} \quad \Psi^{\mathrm{p}}_{\mathrm{iso}} = \text{Eq. (36)} \quad \Psi^{\mathrm{p}}_{\mathrm{kin}} = \text{Eq. (37)}_1 \quad \Psi^{\mathrm{p}}_{\mathrm{dist}i} = \text{Eq. (54)}_2 \tag{68}$$

Accordingly, a neo-Hooke model is used for the elastic response, exponential saturation is considered for isotropic hardening, whereas kinematic and distortional hardening are described by quadratic functions. In order to make the notations comparable, the hardening parameters $\tilde{c}_{\mathrm{kin}}$ and $c_{\mathrm{dis}i}$ are set to

$$\tilde{c}_{\mathrm{kin}} = a_1 \quad c_{\mathrm{dis}i} = A_{1i}. \tag{69}$$

Inserting Eqs. (67)-(69), the evolution equations for distortional hardening (see Eq. (63) and Eq. (65)), the evolution equation for kinematic hardening (see Eq. (60)), an associative evolution equation for isotropic hardening and an associative flow rule into the reduced dissipation inequality (55) eventually yields

$$\begin{aligned} \mathcal{D} \;=\; & \lambda \left(\left[3Q_0^3 + a_2 \left\| \frac{\partial \phi}{\partial \boldsymbol{\Sigma}} \right\| \boldsymbol{Q}_{\mathrm{kin}} : \boldsymbol{Q}_{\mathrm{kin}} \right] \right. \\ & \left. + \|\boldsymbol{\Sigma} - \boldsymbol{Q}_{\mathrm{kin}}\|^2 \left[\underbrace{(\boldsymbol{N}_{\mathrm{r}} : \boldsymbol{Q}_{\mathrm{kin}})\,(\boldsymbol{N}_{\mathrm{r}} \otimes \boldsymbol{N}_{\mathrm{r}}) :: \mathbb{A}_i}_{=:\,R} + \frac{3}{2} A_{2i} \mathbb{A}_i :: \mathbb{A}_i \right] \right) \geq 0. \end{aligned} \tag{70}$$

Again, the positive homogeneity of degree three of the yield function has been applied here, and a summation over i from one to two has to be carried out. By comparing Ineq. (70) to its counterpart (56) of the extended Levkovitch & Svendsen model, it can be seen, that the mathematic structure of dissipation Ineq. (70) is significantly simpler. That is probably due to the thermodynamically consistent structure of the original Feigenbaum & Dafalias model. Only the term R in Ineq. (70) can change its sign. Consequently, a sufficient condition for thermodynamical consistency is $R \geq 0$. However, this condition turned out to be too restrictive for calibrating the model parameters. For this reason, the weaker sufficient condition

$$(\boldsymbol{N}_{\mathrm{r}} : \boldsymbol{Q}_{\mathrm{kin}})\,(\boldsymbol{N}_{\mathrm{r}} \otimes \boldsymbol{N}_{\mathrm{r}}) :: \mathbb{A}_i + \frac{3}{2} A_{2i} \mathbb{A}_i :: \mathbb{A}_i \geq 0. \tag{71}$$

is enforced. With Ineq. (71), a thermodynamically consistent set of material parameters can be determined. However, the enforcement of Ineq. (71) is numerically relatively expensive and strictly speaking, this inequality is only checked for a finite number of loading states. Therefore, thermodynamical consistency cannot be guaranteed for arbitrary loading paths.

3.4. Numerical aspects

The novel constitutive models as presented in Subsections 3.1.2, 3.2.2 and 3.3.2 have been implemented by a state-of-the-art return-mapping scheme, cf. Simo (1998); Simo and Hughes (1998). In this connection, the flow rule has been discretized by an exponential mapping, while the remaining evolution equations have been approximated by means of a backward Euler integration. As a consequence, the resulting scheme is fully implicit and first-order accurate. In contrast to the frameworks Feigenbaum (2008); Noman et al. (2010); Haddadi et al. (2006) based on a co-rotated and hypoelastic framework, the implemented hyperelastoplastic algorithmic formulation shows significant advantages from a physical, as well as from a mathematical point of view, see Simo (1998); Simo and Hughes (1998). Further details are omitted here, but will be discussed in a forthcoming paper.

3.5. Numerical predictions for non-radial loading paths

Although the different distortional hardening models have already been discussed in detail in the previous sections, their precise predictive capabilities cannot be estimated in a straightforward manner. That holds particularly for the novel, more complex extended models suitable for the analysis of magnesium. For this reason, three different loading paths are considered in the present section, i.e.

- uniaxial tension
- uniaxial tension followed by reverse loading
- uniaxial loading followed by uniaxial loading into an orthogonal direction.

For these paths, the mechanical response as predicted by the different constitutive models is analyzed. While the original models are used in Subsection 3.5.1 (reformulated in a hyperelastoplastic framework and a yield surface in terms of Mandel stresses in order to guarantee material frame indifference), the novel extended material models are analyzed in Subsection 3.5.2. For that purpose, the material parameters of the novel models are calibrated for the magnesium alloy AZ31.

3.5.1. The original models of Teodosiu, Levkovitch & Svendsen and Feigenbaum & Dafalias

The fundamental characteristics of the different distortional hardening models according to Feigenbaum (2008); Noman et al. (2010); Haddadi et al. (2006) are briefly presented here. Since the model parameters used in the cited references correspond to different materials, the hardening responses predicted by the models can only be compared qualitatively. However, the final extended models analyzed in

Teodosiu model - Interstitial free mild steel DC06 (1mm), cf. Haddadi et al. (2006)

Q_0 (MPa)	c_{iso}	Q^{∞}_{iso} (MPa)	c_{kin}	$Q^{(0)}_{\text{kin}}$ (MPa)
122.2	27.3	80.0	614.6	6.9

c_{SD}	c_{SD}	S^{∞} (MPa)	n	n_P	r	f	c_P	n_{L}
3.9	1.1	246.7	0	27.7	1.9	0.415	2.2	3.0

Levkovitch & Svendsen model - Ferritic steel LH800, cf. Noman et al. (2010)

Q^{∞}_{iso} (MPa)	c_{iso}	Q^{∞}_{kin} (MPa)	c_{kin}	s_{D}	c_{D}	s_{L}	c_{L}
254.519	4.481	90.896	32.695	0	19.712	-0.863	5.0

Feigenbaum & Dafalias model - Aluminum alloy AU4G T4 (2024), cf. Feigenbaum and Dafalias (2007)

Q_0 (MPa)	κ_1	κ_2 (MPa^{-1})	a_1	a_2 (MPa^{-1})	A_1 (MPa^{-4})	A_2 (MPa^{2})
205	$2 \cdot 10^5$	0.004	$2 \cdot 10^6$	0.015	20	2000

Table 1: Model parameters of the original distortional hardening models

Subsection 3.5.2 are calibrated for the same material. The parameters of the different hardening models are summarized in Tab. 1. Accordingly, an interstitial free mild steel DC06 (1mm), the ferritic steel LH800 as well as the aluminum alloy AU4G T4 (2024) are the materials under investigation.

The mechanical responses obtained from the different constitutive models are shown in Fig. 1 in the form of evolving yield surfaces. Concerning the original Teodosiu model (first row in Fig. 1), isotropic hardening is the most significant hardening mechanism during monotonic loading. If the loading direction is subsequently reversed, the size of the yield surface increases only slowly at first (hardening stagnation). After the strain has reached a certain amplitude, the yield surface increases significantly faster. Similarly, the size of the yield surface changes slowly in the first stage after loading path change for orthogonal loading. However, kinematic hardening is now more pronounced compared to uniaxial loading. Only when the rate of plastic deformation is again aligned with the current loading direction, isotropic hardening is once more the major hardening mechanism. Independently of the loading case, the Teodosiu model cannot predict a distortion of the yield function, since cross hardening is only modeled by modifying isotropic and kinematic hardening.

The evolution of yield surfaces predicted by the original Levkovitch & Svendsen

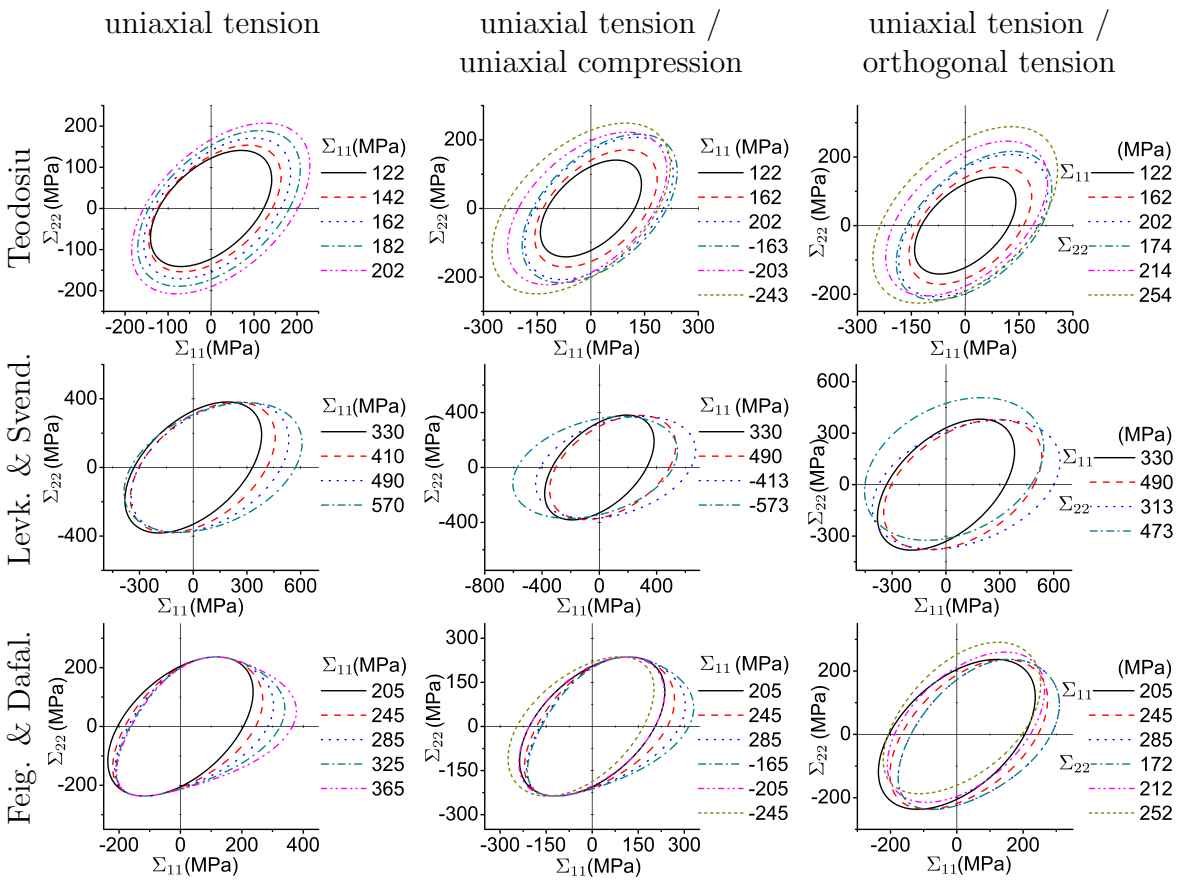

Figure 1: Evolution of the yield surfaces as predicted by the original models proposed by Teodosiu (Haddadi et al., 2006), Levkovitch & Svendsen (Noman et al., 2010) and Feigenbaum & Dafalias (Feigenbaum and Dafalias, 2007). Left to right: monotonic uniaxial tension test; monotonic uniaxial tension test followed by reverse loading (compression); monotonic uniaxial tension test followed by monotonic uniaxial tension into the orthogonal direction

model is shown in the middle row of Fig. 1. For monotonic loading, the yield function becomes distorted with a preferred elongation in loading direction. Since the largest diameter of the initial yield surface is associated with a stress state of the type $\Sigma_{11} = \Sigma_{22}$, the elongation into Σ_{11}-direction during deformation leads to a rotation of the yield surface's principal axes. While the yield surface's diameter increases significantly in loading direction, a small decrease in the orthogonal direction is also seen. The effects observed in the case of uniaxial tension are also present for reverse

loading and orthogonal loading. In sharp contrast to the Teodosiu model, the original Levkovitch & Svendsen model captures the cross hardening effect by a distortion of the yield surface.

Finally, the predictions obtained from the Feigenbaum & Dafalias are analyzed, see bottom row in Fig. 1. As expected by the coupling between kinematic and distortional hardening, the yield surface shows a high curvature in loading direction, whereas it is rather flat in the opposite direction. This effect can be seen for all loadings paths.

3.5.2. The novel extended models calibrated for the magnesium alloy AZ31

Next, the extended distortional hardening models as discussed in Subsection 3.1.2, Subsection 3.2.2 and Subsection 3.3.2 are applied to the modeling of magnesium. The respective model parameters used to capture the mechanical response of the magnesium alloy AZ31 are summarized in the appendix. They have been identified by a standard least square fit. In this connection, loading in three different directions (rolling (RD), transversal (TD) and 45°) has been considered and the numerical predictions have been compared to experimental measurements. Additionally, the r-values atstrain amplitudes of 5% were also included in the model parameter identification. The respective experimental data have been taken from Mekonen et al. (2012). Additional experimental data can be found in Khan et al. (2011). It has to be noted that the considered measurements are not sufficient to identify the model parameters uniquely. For that purpose, additional experiments, which have not been conducted yet, are required. In this respect, the predicted evolutions of the yield functions have to be taken with care.

The predictions of the extended distortional hardening models are shown in Fig. 2. In line with the previous subsection and due to the structure of the underlying equations, the yield function's shape of the extended Teodosiu model does not change. By way of contrast, distortion is predicted by the extended Levkovitch & Svendsen model. Again, a reorientation of the yield function in loading direction can be seen. However, this effect is less pronounced for the magnesium alloy AZ31 compared to the ferritic steel LH800.

While the mechanical response associated with the extended Teodosiu model and the extended Levkovitch & Svendsen model are in line – at least, qualitatively – with the previous subsection, that is not the case for the extended Feigenbaum & Dafalias model. To be more precise and according to Fig. 2, the yield function's curvature is not higher in loading direction compared to the opposite direction for AZ31. A careful analysis of the underlying model parameters reveals that distortional hardening is virtually not active. Hence, the experimentally not observed high curvature

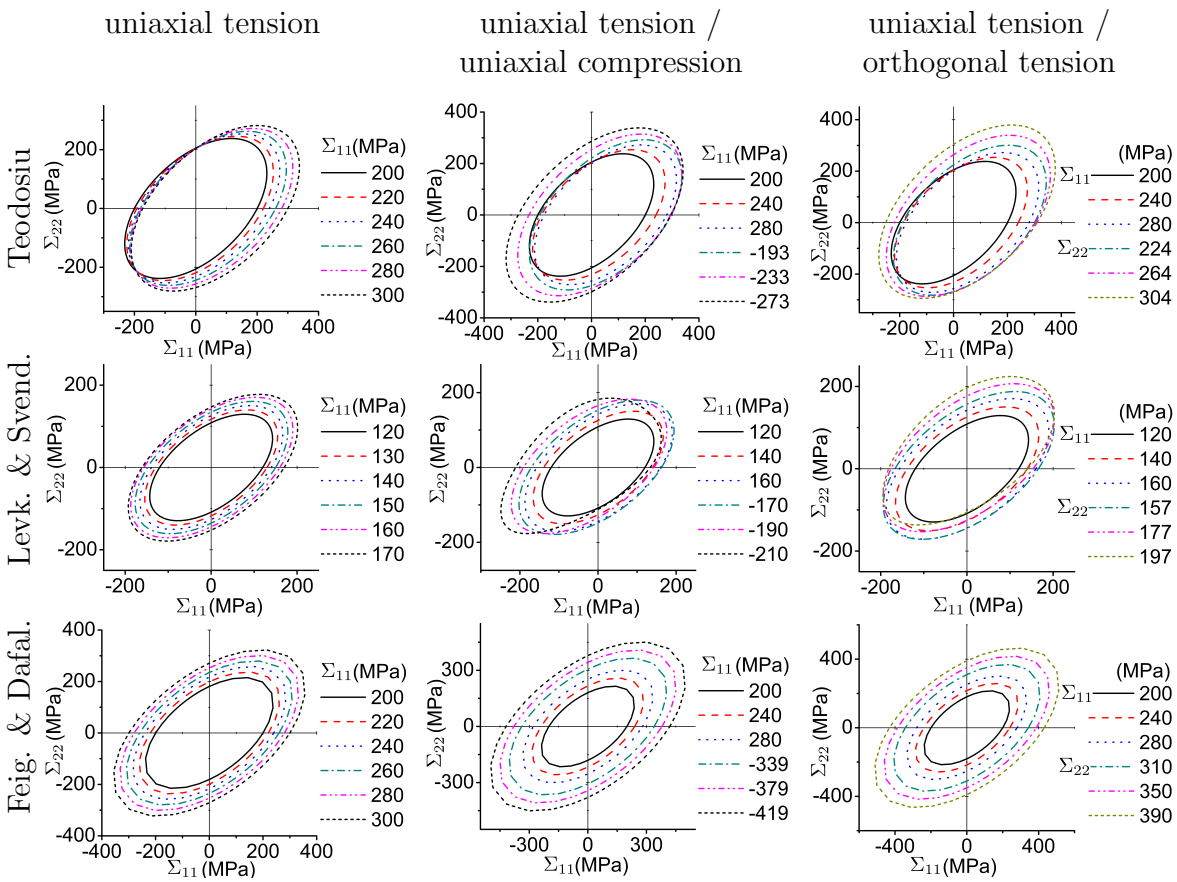

Figure 2: Evolution of the yield surfaces as predicted by the extended models for the magnesium alloy AZ31. Left to right: monotonic uniaxial tension test; monotonic uniaxial tension test followed by reverse loading (compression); monotonic uniaxial tension test followed by monotonic uniaxial tension into the orthogonal direction

in loading direction and the flattening in the opposite direction of the yield function for AZ31 can only be captured by the extended Feigenbaum & Dafalias, if distortion hardening is disabled.

3.6. Final discussion

According to the previous section, the extended Teodosiu, Levkovitch & Svendsen and the Feigenbaum & Dafalias models can capture some of the important mechanical effects observed in magnesium sheets.

Among these models, only the approach originally proposed by Teodosiu and co-workers does not account for a distortion of the yield function, but incorporates cross

hardening by modifying isotropic and kinematic hardening. The unique feature of the Teodosiu model is the precise description of work hardening stagnation, softening and resumption. This description requires a significantly larger number of material parameters compared to the extended Levkovitch & Svendsen and Feigenbaum & Dafalias models. Since focus is on the effect of texture evolution in magnesium sheets, the distortion of the yield surface is the major issue, and thus, the extended Teodosiu model will not be considered in the following.

By way of contrast, the extended Levkovitch & Svendsen model does account for a distortion of the yield surface and, since work hardening stagnation, softening and resumption are not described, the resulting model requires just four material parameters for the evolution equation of distortional hardening. Furthermore, the predictions obtained from the model agree reasonably well with the experimental data. The only, but from the authors' point of view major, drawback is the thermodynamical inconsistency of the model, i.e., it does not fulfill the second law of thermodynamics.

Although the extended Feigenbaum & Dafalias model does not automatically guarantee the fulfillment of the dissipation inequality either, thermodynamical consistency can be enforced through Ineq. (71). Another positive feature is the small number of material parameters which is particularly appealing within the material parameter identification process. The small number of material parameters is related to the fact, that distortional hardening is not decomposed into hardening due to active slip systems and latent slip systems. The only problem associated with the extended Feigenbaum & Dafalias model is that the high curvature of the yield function in loading direction and the flattening in the opposite direction do not seem to fit experimental observations for magnesium alloys, cf. Plunkett et al. (2006). For this reason, the model is not suitable for magnesium alloys - at least not for AZ31.

In summary, there is a need for a novel macroscopic constitutive model able to capture the distortion of the yield function due to texture evolution in magnesium sheets.

4. A novel thermodynamically consistent constitutive model suitable for magnesium alloys

4.1. Fundamentals

The starting point of the novel model is a again the Barlat-type yield function (10). However, in order to normalize the flow rule in advance, the original yield function, which is positively homogeneous of degree three with respect to the relative

stresses, is replaced here by its positively homogeneous of degree one counterpart

$$\phi = \left(J_2^{\frac{3}{2}} - J_3\right)^{\frac{1}{3}} - Q_{\text{iso}} - Q_0. \tag{72}$$

Clearly, by setting $\phi = 0$ it can be seen that both functions essentially span the same space of admissible stresses. Similarly to the extended Levkovitch & Svendsen model (see Subsection 3.2.3), all hardening mechanisms are assumed to be uncoupled leading to the Helmholtz energy

$$\Psi = \Psi^{\text{e}} + \Psi^{\text{p}}_{\text{iso}}(\alpha_{\text{iso}}) + \Psi^{\text{p}}_{\text{kin}}(\boldsymbol{\alpha}_{\text{kin}}) + \Psi^{\text{p}}_{\text{dist1}}(\mathbb{E}_1) + \Psi^{\text{p}}_{\text{dist2}}(\mathbb{E}_2). \tag{73}$$

In this connection and analogously to the previous models, an isotropic neo-Hooke energy is adopted for the elastic response Ψ^{e}, isotropic hardening Ψ_{iso} is captured by an exponential function and, kinematic hardening $\Psi^{\text{p}}_{\text{kin}}$ and distortional hardening $\Psi^{\text{p}}_{\text{dist}i}$ are represented by quadratic functions, i.e.,

$$\Psi^{\text{e}} = \text{Eq. (13)} \quad \Psi^{\text{p}}_{\text{iso}} = \text{Eq. (36)} \quad \Psi^{\text{p}}_{\text{kin}} = \text{Eq. (37)}_1 \quad \Psi^{\text{p}}_{\text{dist}i} = \text{Eq. (54)}_2. \tag{74}$$

The model is completed by suitable evolution equations. Concerning the flow rule, isotropic and kinematic hardening, a convex plastic potential of the type

$$g = \phi + \frac{1}{2}\,\frac{b_{\text{kin}}}{c_{\text{kin}}}\,\boldsymbol{Q}_{\text{kin}} : \boldsymbol{Q}_{\text{kin}} \tag{75}$$

is introduced (see Eq. (16)) leading to

$$\boldsymbol{L}^{\text{p}} = \lambda\frac{\partial g}{\partial \boldsymbol{\Sigma}} = \lambda\frac{\partial \phi}{\partial \boldsymbol{\Sigma}}, \quad \dot{\alpha}_{\text{iso}} = \lambda\,\frac{\partial g}{\partial Q_{\text{iso}}} = \lambda\,\frac{\partial \phi}{\partial Q_{\text{iso}}} = -\lambda, \quad \dot{\boldsymbol{\alpha}}_{\text{kin}} = \lambda\,\frac{\partial g}{\partial \boldsymbol{Q}_{\text{kin}}}. \tag{76}$$

According to Eq. (76), an associative flow rule and an associative evolution equation for isotropic hardening are adopted, whereas an Armstrong-Frederick model is used for kinematic hardening.

In order to derive evolution equations for distortional hardening of the type $\dot{\mathbb{H}}_i = \mathbb{F}(\lambda)$, the similarities between the Teodosiu, the Levkovitch & Svendsen and the Feigenbaum & Dafalias models are recalled. Essentially, all such models postulate an Armstrong-Frederick-type evolution equation for the fourth-order tensor related to cross hardening and the distortion of the yield surface. The only differences are that Teodosiu also considered the effects of work hardening stagnation, softening and resumption and Feigenbaum & Dafalias do not decompose the evolution equation into *dynamic* and *latent* parts, cf. Noman et al. (2010). As is evident from Eq. (75) and Eq. (76) an Armstrong-Frederick-type evolution equation automatically fulfilling the second law of thermodynamics can be designed by means of a plastic potential g

which contains a quadratic term in addition to the yield function. For this reason, distortional hardening can be described by the extended plastic potential

$$g = \phi + \frac{1}{2}\,\frac{b_{\mathrm{kin}}}{c_{\mathrm{kin}}}\,\boldsymbol{Q}_{\mathrm{kin}} : \boldsymbol{Q}_{\mathrm{kin}} + \frac{1}{2}\,\frac{b_{\mathrm{dist1}}}{c_{\mathrm{dist1}}}\,\mathbb{H}_1 :: \mathbb{H}_1 + \frac{1}{2}\,\frac{b_{\mathrm{dist2}}}{c_{\mathrm{dist2}}}\,\mathbb{H}_2 :: \mathbb{H}_2. \tag{77}$$

where $c_{\mathrm{dist}i}$ and $b_{\mathrm{dist}i}$ are model parameters. Due to the additive structure of g, Eqs. (76) are not affected. However, distortional hardening is now consistently included by

$$\dot{\mathbb{E}}_i = \lambda\,\frac{\partial g}{\partial \mathbb{H}_i}, \qquad i \in \{1;2\}. \tag{78}$$

After a lengthy, but nevertheless straightforward calculation, Eqs. (78) can be rewritten as

$$\dot{\mathbb{H}}_1 = \lambda\, b_{\mathrm{dist1}}\,\left[-\frac{1}{4}\,q_1\,J_2^{\frac{1}{2}}\,\left((\boldsymbol{\Sigma}-\boldsymbol{Q}_{\mathrm{kin}})\otimes\boldsymbol{\xi}_1 + \boldsymbol{\xi}_1\otimes(\boldsymbol{\Sigma}-\boldsymbol{Q}_{\mathrm{kin}})\right) - \mathbb{H}_1\right], \tag{79}$$

and

$$\dot{\mathbb{H}}_2 = \lambda\, b_{\mathrm{dist2}}\,\left[\frac{1}{6}\,q_2\,\left((\boldsymbol{\xi}_2\cdot\boldsymbol{\xi}_2)\otimes(\boldsymbol{\Sigma}-\boldsymbol{Q}_{\mathrm{kin}}) + (\boldsymbol{\Sigma}-\boldsymbol{Q}_{\mathrm{kin}})\otimes(\boldsymbol{\xi}_2\cdot\boldsymbol{\xi}_2)\right) - \mathbb{H}_2\right]. \tag{80}$$

with the abbreviation

$$q_i := \frac{c_{\mathrm{dist}i}}{b_{\mathrm{dist}i}}\,\left(J_2^{\frac{3}{2}} - J_3\right)^{-\frac{2}{3}}. \tag{81}$$

In Eqs. (79) and (80), major symmetry of $\mathbb{H}_i$ has been assumed and consistently enforced. Although the structure of Eqs. (79) and (80) looks relatively complex, convexity of g automatically guarantees thermodynamical consistency. In contrast to the extended Feigenbaum & Dafalias model, this holds true, independent of the chosen material parameters for distortional hardening. By using Eq. (77), the dissipation can be conveniently computed in closed form. It eventually results in

$$\mathcal{D} = \lambda\left(2\,Q_0 + Q_{\mathrm{iso}} + \frac{b_{\mathrm{kin}}}{c_{\mathrm{kin}}}\,\boldsymbol{Q}_{\mathrm{kin}} : \boldsymbol{Q}_{\mathrm{kin}} + \frac{b_{\mathrm{dist1}}}{c_{\mathrm{dist1}}}\,\mathbb{H}_1 :: \mathbb{H}_1 + \frac{b_{\mathrm{dist2}}}{c_{\mathrm{dist2}}}\,\mathbb{H}_2 :: \mathbb{H}_2\right) \geq 0 \tag{82}$$

where the positive homogeneity of degree one of the yield function with respect to isotropic, distortional hardening and the relative stresses has been used (for each of the aforementioned variables independently). Clearly, $\mathcal{D}$ is non-negative.

The novel distortional hardening model requires two material parameters ($c_{\mathrm{dist}i}$ and $b_{\mathrm{dist}i}$) for each of the two distortional hardening tensors $\mathbb{H}_i$. The only remaining problem for a model parameter identification arises from the postulated convexity of ϕ, see also Plesek et al. (2010). Within the employed optimization algorithm, a respective constraint has been incorporated.

4.2. Numerical predictions for non-radial loading paths

As in Subsection 3.5.2, the parameters of the novel model have been calibrated by a standard least square approach including the flow curves into RD, TD and 45° direction as well as the r-values at strain amplitudes of 5%. The respective results are shown in Fig. 3. Accordingly, the agreement with respect to the flow curves is

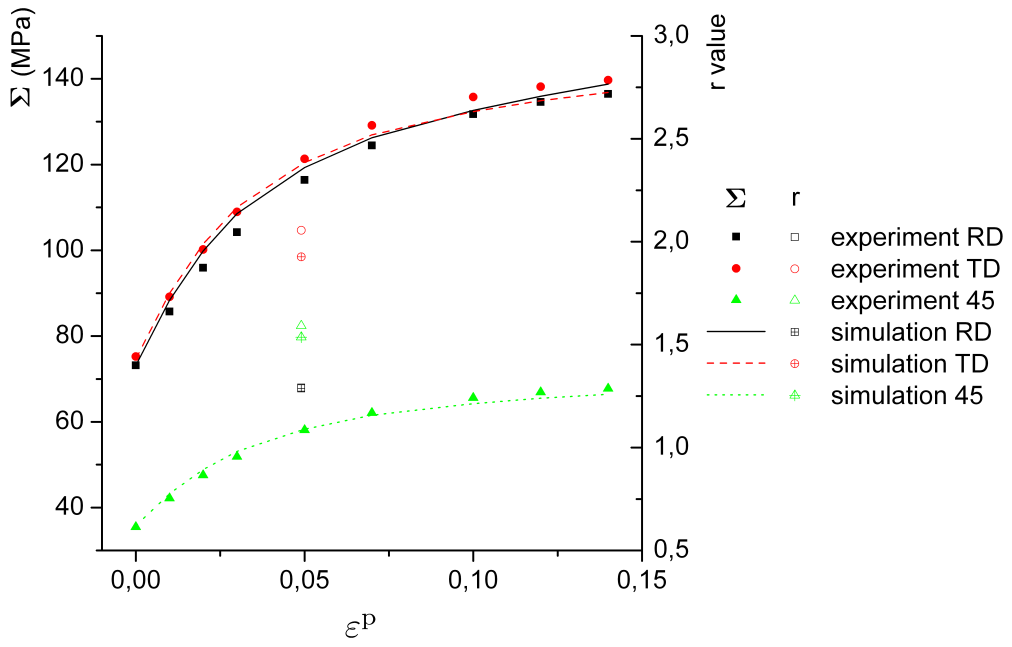

Figure 3: Flow curves for AZ31. Comparison between experiments and predictions by the novel model. The r-values at a strain amplitude of 5% are also included in the diagram

excellent. The r-values are captured reasonably well compared to the predictions by the other extended models (see Subsection 3.5.2).

Based on the calibrated model parameters, the evolution of the yield function during reverse loading and orthogonal loading is computed. It is shown in Fig. 4. For the sake of comparison and since the distortion of the yield function is not very high, the results without distortional hardening are also presented.

The shape change of the yield function can be seen best for the orthogonal loading path. In this case, the principal diameter of the yield surface rotates always

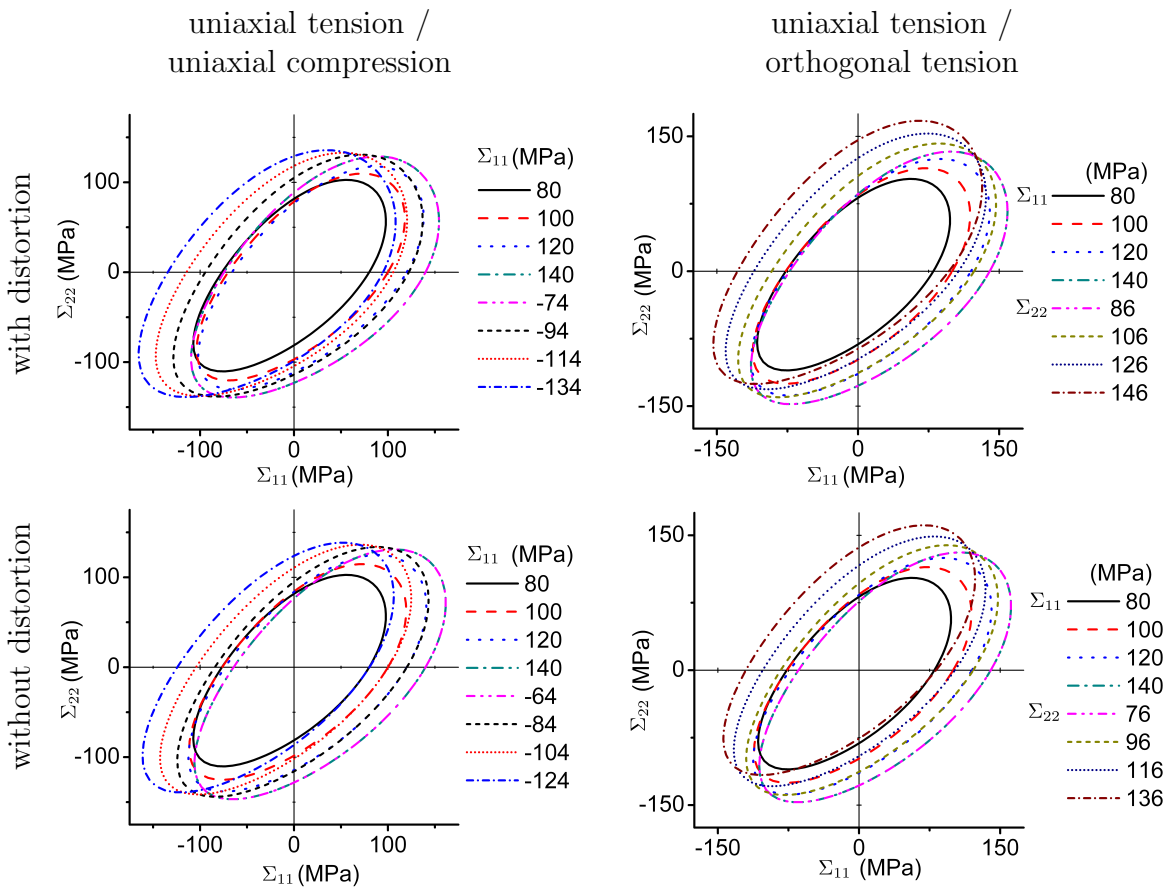

Figure 4: Evolution of the yield surfaces as predicted by the novel model for the magnesium alloy AZ31. Left to right: monotonic uniaxial tension test followed by reverse loading (compression); monotonic uniaxial tension test followed by monotonic uniaxial tension into the orthogonal direction

slightly into the current loading direction, if distortional hardening is accounted for. However, this effect is not very pronounced here. Furthermore, the results have to be interpreted with care due to lack of additional experiments, i.e., yield surface measurements for orthogonal loading are currently not available for AZ31. Nevertheless and in contrast to the models anayzed before, the novel model does capture the evolution of the yield function by simultaneously fulfilling the second law of thermodynamics.

5. Conclusions

In the present paper, different macroscopic phenomenological constitutive models suitable for describing the distortion of the yield function due to texture evolution in polycrystals have been presented. Focus was on the mechanical response of magnesium alloys. Among the existing models, one proposed by Teodosiu and co-workers, one advocated by Levkovitch & Svendsen and one introduced by Feigenbaum & Dafalias were analyzed in detail. It was found that cross hardening and the distortion of the yield function is captured in all models by an evolving fourth-order tensor governed by a differential equation similar to the one of the by now classical Armstrong-Frederick rule. Within the Teodosiu and the Levkovitch & Svendsen model, this evolution equation is decomposed into a part related to currently active slip systems and an additional part that corresponding to latent slip systems. Furthermore, Teodosiu and co-workers focused on the effects of work hardening stagnation, softening and resumption and do not account for a distortion of the yield surface. For a better comparison, all models were reformulated and implemented into the modern frame of hyperelastoplasticity, and a yield function in terms of Mandel stresses was chosen in order to guarantee thermodynamical consistency for elastic processes at finite strain and material frame indifference. Since the original models do not account for the stress differential effect as observed in magnesium alloys, respective extensions were discussed and subsequently implemented. For these extended models, it was shown that only the extended Feigenbaum & Dafalias model can fulfill the second law of thermodynamics by enforcing an additional non-linear inequality. However, that model predicts a high curvature of the yield function in loading direction, while the opposite region of the yield function is rather flat. Since such a response is not observed for most magnesium alloys, a novel constitutive model was presented. The crucial idea was to model distortional hardening similarly to kinematic hardening by an Armstrong-Frederick-type equation obtained from a convex plastic potential, i.e., to apply the framework of generalized standard materials. This procedure automatically guaranteed thermodynamical consistency of the resulting model, independent of the chosen material parameters and for arbitrary loading paths. The predictive capabilities of the final model were eventually demonstrated by comparisons to experimentally measured data.

Acknowledgements

Financial support for the first author was provided by the China Scholarship Council. This funding is gratefully acknowledged.

$$\mathcal{H}_1 = \begin{pmatrix} 6.70 & -8.58 & 1.87 & 0 & 0 & 0 \\ -8.58 & 3.19 & 5.38 & 0 & 0 & 0 \\ 1.87 & 5.38 & -7.26 & 0 & 0 & 0 \\ 0 & 0 & 0 & -14.05 & 0 & 0 \\ 0 & 0 & 0 & 0 & 1 & 0 \\ 0 & 0 & 0 & 0 & 0 & 1 \end{pmatrix} \tag{A.1}$$

$$\mathcal{H}_2 = \begin{pmatrix} -5.77 & -0.78 & 6.56 & 0 & 0 & 0 \\ -0.78 & 2.49 & -1.71 & 0 & 0 & 0 \\ 6.56 & -1.71 & -4.85 & 0 & 0 & 0 \\ 0 & 0 & 0 & -3.02 & 0 & 0 \\ 0 & 0 & 0 & 0 & 1 & 0 \\ 0 & 0 & 0 & 0 & 0 & 1 \end{pmatrix} \tag{A.2}$$

Table A.2: Initial anisotropy of the yield surface - Matrix representations $\mathcal{H}_i$ of the tensors $\mathbb{H}_i$, compare to Mekonen et al. (2012). Since the Mandel stresses are symmetric (isotropic elastic response), $\mathbb{H}_i$ can be represented by 6×6 matrices.

Appendix A. Model parameters for the magnesium alloy AZ31

References

Baltov, A., Sawczuk, A., 1965. A rule of anisotropic hardening. Acta Mechanica 1, 81–92.

Barlat, F., Aretz, H., Yoon, J., Karabin, M., Brem, J., Dick, R., 2005. Linear transfomation-based anisotropic yield functions. International Journal of Plasticity 21 (5), 1009 – 1039.

Barlat, F., Yoon, J., Cazacu, O., 2007. On linear transformations of stress tensors for the description of plastic anisotropy. International Journal of Plasticity 23, 876–896.

Barthel, C., Levkovitch, V., Svendsen, B., 2008. Modeling of sheet metal forming processes taking into account distortional hardening. International Journal of Material Forming 1, 105–108.

Boers, S., Schreurs, P., Geers, M., Levkovitch, V., Wang, J., Svendsen, B., 2010. Experimental characterization and model indentification of directional hardening

Extended Teodosiu model - Subsection 3.1.2

Q_0 (MPa)	c_{iso}	Q_{iso}^{∞} (MPa)	c_{kin}
124.78	107416.15	95.55	-6528.50

$Q_{\text{kin}}^{(0)}$ (MPa)	$\tilde{A}$	$\tilde{B}$	f (MPa)
1546.72	$1.41 \cdot 10^{-2}$	$-1.17 \cdot 10^{-2}$	0.57

Extended Levkovitch & Svendsen model - Subsection 3.2.2

Q_{iso}^{∞} (MPa)	c_{iso}	Q_{kin}^{∞} (MPa)	c_{kin}
96.09	155764.85	1019.76	101.20

s_{D1}	c_{D1}	s_{L1}	c_{L1}	s_{D2}	c_{D2}	s_{L2}	c_{L2}
948.10	-0.014	1029.27	-0.0033	1746.09	0.99	987.01	1.10

Extended Feigenbaum & Dafalias model - Subsection 3.3.2

Q_0 (MPa)	κ_1	κ_2 (MPa^{-1})	a_1	a_2 (MPa^{-1})
115.47	$2.975 \cdot 10^{8}$	$9.37 \cdot 10^{-4}$	102437.7	0.0015

A_{11} (MPa^{-4})	A_{21} (MPa^{2})	A_{12} (MPa^{-4})	A_{22} (MPa^{2})
0.826	2029.1	-0.00003	1995.3

Novel constitutive model - Subsection 4

Q_0 (MPa)	Q_{iso}^{∞} (MPa)	c_{iso}	b_{kin}	c_{kin} (MPa)
611.90	798.16	288.05	171.53	521.89

b_{dist1}	c_{dist1} (MPa^{-1})	b_{dist2}	c_{dist2} (MPa^{-1})
0.001869	0.774	0.003482	2.094

Table A.3: Model parameters for the magnesium alloy AZ31. The elasticity constants are $E = 45000$ (MPa) and $\nu = 0.35$.

effects in metals for complex strain path changes. International Journal of Solids and Structures 47, 1361–1374.

Bruhns, O., Xiao, H., Meyers, A., 1999. Self-consistent eulerian rate type elasto-plasticity models based upon the logarithmic stress rate. International Journal of Plasticity 15 (5), 479 – 520.

Cazacu, O., Barlat, F., 2004. A criterion for description of anisotropy and yield differential effects in pressure-insensitive metals. International Journal of Plasticity 20, 2027–2045.

Choi, S.-H., Kim, D., Seong, B., Rollett, A., 2011. 3-D simulation of spatial stress distribution in an AZ31 Mg alloy sheet under in-plane compression. International Journal of Plasticity 27 (10), 1702 – 1720.

Christian, J., Mahajan, S., 1995. Deformation twinning. Progress in Materials Science 39 (1-2), 1–157.

Coleman, B., Gurtin, M., 1967. Thermodynamics with internal state variables. Journal of Chemical Physics 47, 597–613.

Feigenbaum, H., 2008. Directional distortional hardening in plasticity based on thermodynamics. Ph.D. thesis, University of California Davis.

Feigenbaum, H., Dafalias, Y., 2007. Directional distortional hardening in metal plasticity within thermodynamics. International Journal of Solids and Structures 44, 7526–7542.

Feigenbaum, H., Dafalias, Y., 2008. Simple Model for Directional Distortional Hardening in Metal Plasticity within Thermodynamics. Journal of Engineering Mechanics 134 (9), 730–738.

Fernandez, A., Prado, M. T. P., Wei, Y., Jerusalem, A., 2011. Continuum modeling of the response of a Mg alloy AZ31 rolled sheet during uniaxial deformation. International Journal of Plasticity 27 (11), 1739–1757.

Haddadi, H., Bouvier, S., Banu, M., Maier, C., Teodosiu, C., 2006. Towards an accurate description of the anisotropic behaviour of sheet metals under large plastic deformations: Modelling, numerical analysis and indentification. International Journal of Plasticity 22, 2226–2271.

Hiwatashi, S., Bael, A., Houtte, P., Teodosiu, C., 1998. Prediction of forming limit strains under strain-path changes: application of an anisotropic model based on texture and dislocation structure. International Journal of Plasticity 14 (7), 647–669.

Homayonifar, M., Mosler, J., 2011. On the coupling of plastic slip and deformation-induced twinning in magnesium: A variationally consistent approach based on energy minimization. International Journal of Plasticity 27, 983–1003.

Homayonifar, M., Mosler, J., 2012. Efficient modeling of microstructure evolution in magnesium by energy minimization. International Journal of Plasticity 28, 1–20.

Johansson, G., Ekh, M., Runesson, K., 2005. Computational modeling of inelastic large ratcheting strains. International Journal of Plasticity 21 (5), 955 – 980.

Khan, A. S., Pandey, A., Gnäupel-Herold, T., Mishra, R. K., 2011. Mechanical response and texture evolution of AZ31 alloy at large strains for different strain rates and temperatures. International Journal of Plasticity 27 (5), 688 – 706.

Lebensohn, R., Liu, Y., Castaneda, P. P., 2004. On the accuracy of the self-consistent approximation for polycrystals: comparison with full-field numerical simulations. Acta Materialia 52 (18), 5347 – 5361.

Lee, E., 1969. Elastic-plastic deformation at finite strains. Journal of Applied Mechanics 36, 1–6.

Lemaitre, J., 1985. A continuous damage mechanics model for ductile fracture. J. Eng. Mat. Techn. 107, 83–89.

Li, S., Hoferlin, E., Bael, A., Houtte, P., Teodosiu, C., 2003. Finite element modeling of plastic anisotropy induced by texture and strain-path change. International Journal of Plasticity 19, 647–674.

Ma, Q., Kadiri, H. E., Oppedal, A., Baird, J., Li, B., Horstemeyer, M., Vogel, S., 2012. Twinning effects in a rod-textured AM30 magnesium alloy. International Journal of Plasticity 29, 60 – 76.

Mandel, J., 1971. Plasticite classique et viscoplasticitite. CISM.

Mekonen, M. N., Steglich, D., Bohlen, J., Letzig, D., Mosler, J., 2012. Mechanical characterization and constitutive modeling of mg alloy sheets. Materials Science and Engineering: AIn press, http://dx.doi.org/10.1016/j.bbr.2011.03.031.

Miehe, C., Rosato, D., 2007. Fast texture updates in fcc polycrystal plasticity based on a linear active-set-estimate of the lattice spin. Journal of the Mechanics and Physics of Solids 55 (12), 2687 – 2716.

Miehe, C., Schotte, J., Lambrecht, M., 2002. Homogenization of inelastic solid materials at finite strains based on incremental minimization principles. application to the texture analysis of polycrystals. Journal of the Mechanics and Physics of Solids 50 (10), 2123 – 2167.

Mosler, J., 2010. Variationally consistent modeling of finite strain plasticity theory with non-linear kinematic hardening. Computer Methods in Applied Mechanics and Engineering 199, 2753–2764.

Neil, C. J., Agnew, S. R., 2009. Crystal plasticity-based forming limit prediction for non-cubic metals: Application to mg alloy AZ31B. International Journal of Plasticity 25 (3), 379 – 398.

Noman, M., Clausmeyer, T., Barthel, C., Svendsen, B., Huetink, J., Riel, M., 2010. Experimental characterization and modeling of the hardening behavior of the sheet steel LH800. Materials Science and Engineering A 527, 2515–2526.

Ogden, R., 1997. Non-Linear Elastic Deformations. Dover Publications.

Peeters, B., Kalidindi, S., Teodosiu, C., Houtte, P., Aernoudt, E., 2002. A theoretical investigation of the influence of dislocation sheets on evolution of yield surfaces in single-phase B.C.C. polycrystals. Journal of the Mechanics and Physics of Solids 50, 783–807.

Pietryga, M. P., Vladimirov, I. N., Reese, S., 2012. A finite deformation model for evolving flow anisotropy with distortional hardening including experimental validation. Mechanics of Materials 44 (0), 163 – 173.

Plesek, J., Feigenbaum, H., Dafalias, Y., 2010. Convexity of Yield Surface with Directional Distortional Hardening Rules. Journal of Engineering Mechanics 136 (4).

Plunkett, B., Lebensohn, R., Cazacu, O., Barlat, F., 2006. Anisotropic yield function of hexagonal materials taking into account texture development and anisotropic hardening. Acta Materialia 54 (16), 4159 – 4169.

Simo, J., Hughes, T., 1998. Computational Inelasticity. Vol. 7 of Interdisciplinary Applied Mathematics. Springer-Verlag New York, Inc.

Simo, J. C., 1998. Numerical analysis of classical plasticity. Vol. IV of Handbook for numerical analysis. Elsevier, Amsterdam.

Vladimirov, I. N., Pietryga, M. P., Reese, S., 2010. Anisotropic finite elastoplasticity with nonlinear kinematic and isotropic hardening and application to sheet metal forming. International Journal of Plasticity 26 (5), 659 – 687.

Wang, J., Levkovitch, V., Reusch, F., Svendsen, B., Huetink, J., Riel, M., 2008. On the modeling of hardening in metals during non-proportional loading. International Journal of Plasticity 24, 1039–1070.

Wang, J., Levkovitch, V., Svendsen, B., 2006. Modeling and simulation of directional hardening in metals during non-proportional loading. Journal of Materials Processing Technology 177, 430–432.

Xiao, H., Bruhns, O., Meyers, A., 2000. A consistent finite elastoplasticity theory combining additive and multiplicative decomposition of the stretching and the deformation gradient. International Journal of Plasticity 16 (2), 143 – 177.